LUND UNIVERSITY
Faculty of Science

Studies of Dark Showers for Present and Future Colliders

Nicoline Krogh Hemme

Thesis submitted for the degree of Master of Science

Project duration: 10 months

Examination: June 2022

Supervised by Caterina Doglioni & Suchita Kulkarni

Department of Physics
Division of Particle Physics
June 2022

Abstract

In this work we explore a strongly-interacting dark sector with a Z' portal to the Standard Model. We focus on the dark shower phenomenology and their semi-visible jet signatures with a strong emphasis on first principles of the theory. We use PYTHIA and DELPHES for event generations and detector simulations, and consider both pp and e^+e^- collision events at 13 TeV. The kinematic studies are based on jet objects with radius $R = 0.4$ or $R = 0.8$. This work highlights important model parameters and studies correlations between several of these parameters and the kinematics of dark shower models. Additionally, we take a closer look at the r_{inv} parameter that is commonly used in semi-visible jet studies and propose a new variable, r_{rec}, based on event energy. This new variable is realistically observable and shows a strong correlation to r_{inv} in e^+e^- collision events.

Acknowledgements

I want to thank Caterina Doglioni for introducing me to this field and topic. This project opened the door to a very exciting field full of talented and kind people, and it has truly been a pleasure to be a part of it for the past year. One year ago, I did not know exactly what path to take in physics, but through this opportunity you have granted me, I have realised exactly where I fit in. I am truly grateful to you for leading me here.

I also want to thank Suchita Kulkarni for having been such a great mentor throughout working on this project. You have pushed me to work harder, but been supportive when needed, and I believe you have a gift to motivate and inspire people because I always left our meetings with newfound motivation.

I cannot mention inspiration without mentioning the one thing I found most inspirational on my journey with this project; to be working so closely with two amazing women in science. I hope we will work together again in the future, and I hope that we will continue to see women thrive in the field.

Contents

1 Introduction

In the past century our understanding of the Universe has evolved tremendously. While we have developed an impressively well validated Standard Model of particle physics [1], we have also learned that there are many things we do not know or understand about the Universe. One of the biggest mysteries of the Universe today is the mystery of dark matter. The matter content of the Universe that we can explain by the Standard Model only makes up $\sim 16\%$ of all the matter content in the Universe [2]. The rest is made up of dark matter.

Dark matter was first postulated by the Swedish astronomer Knut Lundmark in 1930 [3], and today the existence of dark matter is indisputable. The general consensus is that dark matter is a new and exotic particle that we have not yet discovered which neither emits nor reflects light. There is an infinite number of theories of what kind of particle dark matter could be. No theory has yet been proven, and it is generally very difficult or even impossible with our current knowledge and technology to disprove most theories.

The theory that is explored in this thesis is that of a confined dark sector [4]. The term *dark sector* can be described as a sector consisting of several new particles that are all invisible to our detectors, i.e. dark particles. This dark sector may be able to interact with the Standard Model through some portal, and if so, we may be able to detect the results of such interactions. This theory of dark matter can be thought of as a collection of dark quarks that can interact strongly with each other but not with the Standard Model quarks. The portal can be a new massive boson that can interact both with the Standard Model and the dark sector.

This type of theory allows for very interesting phenomenology in a high-energy particle collision, such as those carried out at the Large Hadron Collider (LHC). Due to the strong interactions between the dark quarks, a high-energy particle collision may result in a parton shower similar to that seen for Standard Model quarks, where many new dark particles are created. This is called a *dark shower*. In recent years several studies have been made on the collider signatures of these dark showers and show promising results for our ability to discover these signatures, see e.g. Refs. [5, 6, 7]. Nonetheless, very little research into dark showers has been carried out on real collider data, and only very recently was the first collider search for a strongly interacting dark sector published [8]. This thesis will continue the exploration of dark showers with the goal to expand our understanding of dark showers and provide motivation for further studies and searches of dark shower signatures.

2 Theory

2.1 The Standard Model of Particle Physics

The Standard Model of Particle Physics (SM) is a well-motivated and well-tested theory [1] that describes the elemental particles and forces that we have observed in our Universe. The model provides the basis for our understanding of ordinary matter. It includes quarks and leptons as well as their antiparticles, the Higgs boson and the force carriers of 3 of the 4 fundamental forces; the strong force, the electromagnetic force and the weak force. The latter two are parts of a more fundamental interaction named the electroweak interaction [9]. The fourth fundamental force is the gravitational force, which has not yet been successfully incorporated into the SM. This force interacts with any massive particle. The Standard Model is depicted in Fig. 2.1, where the properties mass and charge can be found for each elemental particle and force carrier.

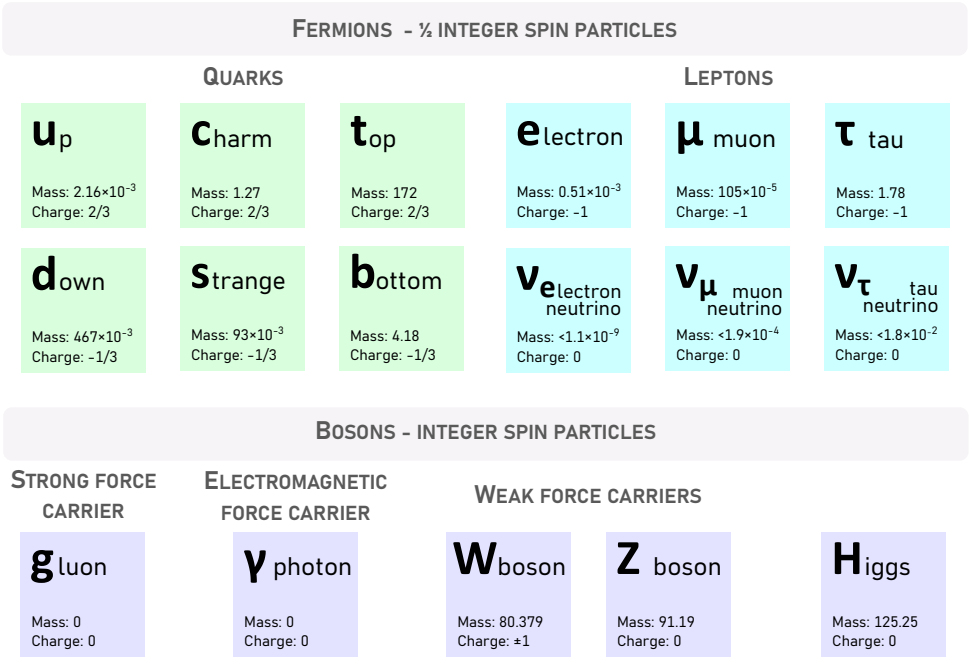

Figure 2.1: The Standard Model of Particle Physics. Masses are given in units of GeV/c^2 and charges in units of e. The values have been sourced from Ref. [10].

All fermions are half-integer spin particles that obey Fermi-Dirac statistics and the Pauli exclusion principle that states that *no 2 fermions can occupy the same quantum state* (see e.g. Ref. [11] for more details on the Pauli exclusion principle). The distinctive difference between quarks and leptons is that quarks carry a color charge, enabling them to interact strongly, whereas leptons do not carry a color charge and cannot interact strongly. The strong interactions and the color symmetry will be elaborated upon in the section below. Both quarks and leptons can interact weakly and electromagnetically.

There are 6 different kinds of quarks, the *up*, *down*, *charm*, strange, *top* and *bottom* quark. These are also known as flavors and the number is denoted N_f. Leptons only come in 3 flavors, the *electron*, the μ and the τ, and they each have an associated neutrino. The neutrinos have zero electric charge and very low masses. They interact very weakly with matter and have for many years escaped collider detectors without leaving any trace of their interactions[1], despite being abundantly produced in particle collision events [14]. They are therefore always present in the SM background.

2.1.1 QCD and Hadronization

The strong interactions between the quarks and gluons are described by an $SU(3)_C$ color symmetry group. This theory is named Quantum Chromodynamics or QCD for short. Color describes a charge different from the electric charge and is an additional quantum number. There are 3 colors, as signified by the 3 in $SU(3)_C$, and the number of colors is denoted N_c. The quarks can carry one of the three colors. The colors are usually known as red, green and blue, and anti-quarks can carry an anti-red, anti-green or anti-blue color charge.

A special property of QCD is that below some energy scale Λ_{QCD}, the massive particles of the theory, i.e. the quarks, are always bound together in a configuration that is colorless. This property is called confinement [15] and Λ_{QCD} is called the QCD confinement scale and is of the order of a few hundred MeV [16]. The interaction energy between color charges, such as a red quark and an anti-red anti-quark, increases linearly with distance at large distances, approximately when the energy of the system falls below the confinement scale. At one point the interaction energy becomes so large that it is energetically favourable to create a new pair of quarks from the vacuum. In this example, it will be a new anti-red anti-quark to bind with the red quark and a new red quark to bind with the anti-red anti-quark. This process is called hadronization.

In the opposite energy limit, i.e. when the energies of the system are above the confinement scale, the QCD theory exhibits a behaviour known as asymptotic freedom. As the system energy increases, the interaction strength decreases and asymptotically approaches a point where it effectively vanishes. This requires an extremely high energy density, but is achievable in high-energy particle collision at colliders such as the LHC [17].

The colorless configuration mentioned earlier, the quark and anti-quark, is called a meson and is one of the most common types of colorless configurations. The other common type is the baryon, which consists of 3 quarks (or 3 anti-quarks), one of each color, which

[1]The first collider neutrinos have recently been detected at a pilot run in 2018 of the FASER neutrino detector [12] at the LHC [13].

together makes a colorless configuration. The collective name for mesons and baryons (as well as other types of colorless configurations) is hadrons, hence the name hadronization given to the process of hadron-creation.

Hadronization is a key component of high-energy collision events. The process of hadronization is initiated when quarks and gluons are created in the collision event, and the energy in the system is high enough to give rise to a *shower* of new particles. Often this shower of new particles will be collimated and there will be multiple of these collimated showers. This is due to the is conservation of transverse momentum. If the $q\bar{q}$ pair is created from particles with transverse momentum, the new pair will generally travel along this direction, resulting in the collimation of the shower. If a $q\bar{q}$ pair is created from particles with no transverse momentum, the q and $\bar{q}$ will travel in opposite directions to each other, resulting in two separate and back-to-back showers.

A collection of collimated hadronic momenta is called a *jet* and is extensively used in high-energy particle collisions to understand the dynamics of the event and subsequent hadronization process [18]. The general idea of a jet algorithm is to cluster particles that are nearby each other into a single 4-momentum object, i.e. the jet [19]. Jets can be reconstructed from any kind of four-momentum using specific algorithms [20], and in this work we focus on jets built from the simulated energy depositions in the detector or built from stable final-state generator-level particles. In general, a jet will have a characteristic size, or radius R, that in the case of the anti-k_t algorithm [20] is related to the maximum distance between clustered particles. Usually the jet algorithm is more complex and takes into account more factors than the distance between particles, such as the momenta of the particles to cluster soft particles with hard particles rather than alone in a soft-particles-only jet.

2.2 Dark Matter

While the SM particles make up everything that we understand as ordinary matter, such as the Earth and ourselves, ordinary matter only makes up about $\sim 16\%$ of all the matter content in the Universe. The remaining $\sim 84\%$ is the relic dark matter abundance, a term used to describe the relic abundance of matter in the Universe that can seemingly not be explained by the SM. This composition of matter in the Universe is well-established [2], but the composition of the dark matter itself remains a mystery.

The existence of dark matter was first postulated in 1930 by the Swedish astronomer, Knut Lundmark while he was working at Lund University. By comparing the mass of galaxies deduced from their luminosity to the mass deduced from the velocity dispersion of those galaxies, he was able to prove that there is far more mass within the galaxies than what we can see [3]. He wrote in his paper, without much concern or quandary, that this discrepancy was due to "dunkle Materie" (dark matter) that was missing from the luminosity calculations. Interestingly, he did not claim that this was some sort of new, exotic matter but mentioned that the dark matter could consist of extinguished stars, dust, meteors and such. Other astronomers found similar discrepancies in the following years, including Fritz Zwicky in 1933 [21].

While the term dark matter had been used since 1930, it was only much later, in the 1970s, that the term began to take on an important role in physics and cosmology. This came after a realisation that only if galaxies contained much more mass than what could be observed, could galaxies remain stable and the Universe be closed, a geometry of the Universe that was at the time believed to be the true geometry of the Universe [22, 23]. It was also around this time that it was proposed that dark matter was some type of *hidden* matter [24], rather than faint objects.

Since then, many explanations for dark matter have been proposed and many experiments have been devoted to detect dark matter, and yet, ∼50 years later, dark matter has not been detected and no theory of dark matter has been proven. Perhaps the most well-known theory of dark matter is that it is made of Weakly Interacting Massive Particles (WIMPs) [25]. Such a type of particle would be able to interact weakly with SM particles but would remain invisible to our detectors, thus they may be produced in particle collisions and escape the detectors as invisible energy. A great motivation for the WIMP theory is that WIMPs in general provide a dark matter candidate that can account fully for the relic dark matter abundance [21]. Indeed some theories are only able to account for parts of the dark matter density, such as the Massive Astrophysical Halo Objects (MACHO) theory [26, 27] and require additional dark matter candidates to make up the relic dark matter abundance. Despite the popularity of the WIMP theories no experiments have so far been able to conclusively prove the existence of such a dark matter candidate (see e.g. Refs. [28, 29, 30, 31]). With consistent null results from WIMP searches, the interest has grown for other dark matter candidates. One of these theories, which is the focus of this thesis, is the strongly-interacting dark sector theory.

2.3 Introduction to Strongly-interacting Dark Sectors

The idea of a dark sector (DS) is the idea that there may exist a whole sector of undiscovered particles and possibly unknown forces. Naturally, there are many possible ways to imagine such a dark sector, or a *hidden valley* (HV) as it can also be referred to. Generally, a HV refers to an extension of the SM by some new gauge group that may be able to communicate with the SM through some new mediator or *portal* [32]. This thesis explores the phenomenology of a dark sector arising from the introduction of a new confining group, an $\mathrm{SU}(\mathrm{N}_D)$ group, where the subscript D signifies the number of dark colors, and new particles charged under this group. Below a characteristic energy scale, named Λ_D in correspondence to the QCD confinement scale, the new particles, referred to as *dark quarks*, confine into composite particles similar to hadrons and are called *dark hadrons*. These composite particles generally include dark matter candidates [33], making such a theory an interesting extension to the SM. With the additional requirement for the group to exhibit asymptotic freedom, such dark sector theories are known as QCD-like dark sectors or strongly-interacting dark sectors.

The dark quarks are assumed to be neutral under the SM gauge group. Similarly the SM particles are assumed to be neutral under the new $\mathrm{SU}(\mathrm{N}_D)$ group, such that the dark particles cannot interact directly with the SM particles and forces. They can, however,

Figure 2.2: What if there exists a whole sector of particles we have not discovered yet?

interact indirectly if introducing a portal between the SM and the DS. The portal assumed in this work is a new massive vector boson, denoted Z'. The Z' boson can couple to the DS quarks and the SM quarks. In some theories the Z' boson can also couple to leptons. This is characterised by whether the Z' is leptophobic or not.

The number of flavors in the new SU(N_D) group is denoted N_{f_D}. A theory with N_{f_D} mass degenerate quarks that can confine into $N_{f_D}^2 - 1$ spin-0 mesons, namely dark pions π_D, and $N_{f_D}^2 - 1$ spin-1 mesons, namely dark rho mesons ρ_D. Additionally, the theory contains a spin-0 singlet, η'_D, and spin-1 singlet, ω_D.

Models of a strongly-interacting dark sector with a portal to the SM can contain very interesting phenomenology that may be observed at collider experiments. While there are several interesting signatures that can be considered, the focus of this thesis is on the phenomenology of dark showers and their signatures semi-visible jets.

2.3.1 Dark Showers and Semi-visible Jets

If there exists dark quarks that due to their QCD-like interaction can give rise to the creation of additional dark quarks in high energy systems, it would be expected that such systems could cause a QCD-like shower within the DS, i.e. a dark shower. A dark shower could potentially occur in particle collisions at the LHC if there is a portal between the SM and DS. If at least some of the dark particles are unstable, they may even decay back to the SM through the portal, leaving behind visible signatures. A distinct signature of dark showers is the *semi-visible jet*. The semi-visible jet is characterised as a jet in which some (or all) of the visible constituents originate from the decays of DS particles. Indeed, semi-visible jets could have already been present at the LHC, but we simply haven't looked for them yet.

The invisibility of the dark shower is often characterized by the parameter r_{inv}, defined as

$$r_{\text{inv}} = \left\langle \frac{N_{\text{stable dark hadrons}}}{N_{\text{stable dark hadrons}} + N_{\text{unstable dark hadrons}}} \right\rangle \tag{2.1}$$

Roughly speaking, there are three distinct r_{inv} scenarios:

r_{inv} = 1 - the fully invisible dark shower
In this scenario, $N_{\text{unstable dark hadrons}} = 0$ so all dark hadrons are stable and remain invisible. The signature of such a dark shower is expected to be a mono-jet; none of the particles of the dark shower can be detected, but if an initial-state-radiation jet occurs in connection with the dark particles, the event is expected to have a high p_T jet in one direction and missing transverse energy, also denoted MET or $\not{E}_{\text{T}}$, in the opposite direction. This signature is also what is expected from the WIMP theory, and indeed the signatures would be indistinguishable [34].

r_{inv} = 0 - the fully visible dark shower
The fully visible shower requires all dark hadrons to be unstable and to only contain SM final-state particles. The signatures of such dark showers are particularly tricky, as they will generally look much like a QCD shower [34]. Nonetheless, the showers are expected to contain traces of non-QCD origin in their substructure, see e.g. References [6] and [35] for further details and studies on jet substructures related to dark showers.

r_{inv} between 0 and 1 - the semi-visible dark shower
This intermediate scenario is the one assumed in this thesis. It requires that only some and not all dark hadrons decay to the SM. As some dark hadrons remain stable, some $\not{E}_{\text{T}}$ is expected to appear in the event, and more specifically, the $\not{E}_{\text{T}}$ is expected to align very closely with a jet. When the two initial dark quarks travel in opposite directions and subsequently each results in a dark shower, the showers are said to be back-to-back and will have an angular separation of approximately $\Delta\phi \sim \pm\pi$. Assuming that a lot of energy will be carried in the dark showers, which is a fair assumption when the portal boson is heavy, the semi-visible dark showers will leave a semi-visible jet signature. Additionally, since there are frequent fluctuations in the kinds of dark quarks created and the multiplicity of each, i.e. the amount of each quark, there will be fluctuations in the amount of various hadrons produced. Therefore, one dark shower will likely contain more stable dark hadrons than the opposite dark shower, thus being more invisible. This results in the specific semi-visible dark shower signature; two back-to-back jets with the $\not{E}_{\text{T}}$ aligned closely with one of the two jets, i.e. $\Delta\phi_{\text{J},\not{E}_{\text{T}}} \sim 0$, where the subscript J signifies the jet that aligns best with the $\not{E}_{\text{T}}$.

The back-to-back semi-visible jet signature is particularly interesting, as the $\Delta\phi_{\text{J},\not{E}_{\text{T}}} \sim 0$ region is discarded in most standard searches at the LHC due to a high QCD background in this region [34], and so the signatures could indeed be hiding in LHC collisions.

A common method used in particle collider experiments to find and identify a new resonance particle, which is a very short-lived particle such as a heavy boson, is to perform a resonance search, also known as a bump hunt. The resonance search utilises the variable *invariant mass* defined as

$$M_{JJ}^2 = (p_{J1} + p_{J2})^2 \tag{2.2}$$

where p_{J1} and p_{J2} are the momenta of the leading and sub-leading jets, respectively. If the resonance particle decays on-shell, i.e. it obeys the energy-momentum relation $E^2 = p^2 + m^2$ (in natural units), and the decay products initiate the leading and sub-leading jet, then the invariant mass will give back the rest mass of the resonance particle. The resonance particle can also decay off-shell which will cause the resultant invariant mass to deviate from the rest mass. Additionally, background noise and other participants

of the events will alter the resultant invariant mass. The value will fluctuate from event to event. However, over a large number of events, a peak - or a bump - in the invariant mass distribution is expected to appear at the rest mass of the resonance particle. This method led to the discovery of the Higgs boson in 2012 [36]. It is natural to assume that if another heavy boson exists it is likely to be discovered through a resonance search as well. In the case of a semi-visible dark shower, however, a resonance search like this may not yield any clear results. The reason is that if there are stable dark particles in the event, the momenta of these particles will be in the $\not{E}_{\mathrm{T}}$ and will not contribute to the invariant mass. The invariant mass will be smaller than rest mass even if the Z' boson decays on-shell. Furthermore, the ratio of stable dark hadrons in the dark shower will fluctuate from event-to-event, which can be represented as event-by-event fluctuations in r_{inv}, and so the $\not{E}_{\mathrm{T}}$ caused by dark particles will differ between events as well. Taking these factors into account, the variable *transverse mass* was proposed in Ref. [37] to be utilised instead and is defined as

$$M_T = M_{JJ}^2 + 2\big(\sqrt{M_{JJ}^2 + p_{T_{JJ}}^2}\not{E}_{\mathrm{T}} - \vec{p}_{T_{JJ}} \cdot \vec{\not{E}}_{\mathrm{T}}\big) \tag{2.3}$$

where $\vec{p}_{T_{JJ}}$ is the vector sum of the transverse momentum vectors of the leading and sub-leading jets. The transverse mass includes the $\not{E}_{\mathrm{T}}$ and has shown to be very useful for resonance searches of semi-visible di-jet events with r_{inv} in the intermediate region, while the invariant mass still performs well at $r_{\mathrm{inv}} \sim 0$ [5, 34].

This thesis will study both the invariant and transverse mass of various dark shower models, but will consider many more kinematic variables.

3 Simulation Tools

The simulation of particle collision events is a key component of this thesis and most of the results are based upon these simulations. The tools used are PYTHIA [38] and DELPHES [39], versions 8.307 and 3.5.0, respectively. The data from these simulations are analysed and later plotted in Python scripts that rely on the utilisation of ROOT [40] tools. These scripts have been built up using an existing framework, and are publicly available on GitHub, see Ref. [41]. A schematic of the general process is illustrated in Fig. 3.1. In this section, the tools PYTHIA and DELPHES are briefly introduced. The aspects of the tools relevant for this thesis are further elaborated upon.

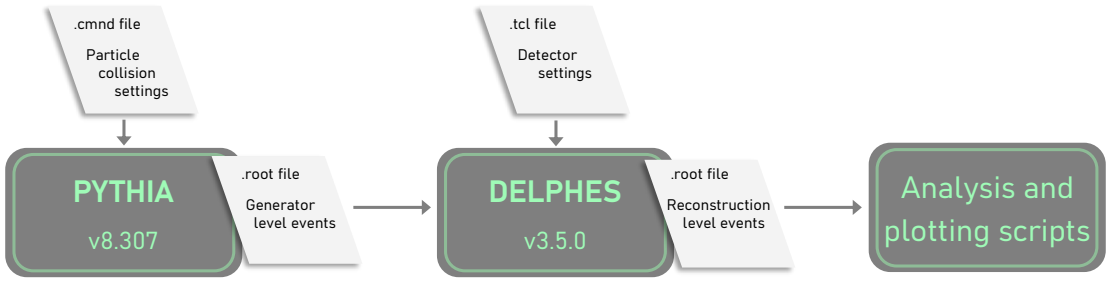

Figure 3.1: The routine for analysing models.

During the introduction of the simulation tools, the terms generator-level and reconstruction-level will be used. Generator-level refers to information from the event generator PYTHIA, which does not take into account the effects and limitations of a detector. This information will therefore contain every single particle included in the event, even invisible ones, and their precise information, such as where they were produced and, if they are unstable, how they decayed. This is also sometimes referred to as truth-level. Reconstruction -level refers to the output of the detector simulator, in this case DELPHES. In the detector simulator, only certain events and particles will be stored. Events not fulfilling the trigger requirements, or particles that are invisible or interact very little with the detector will not be stored. The reconstruction-level information will also not contain any information of the particle origin aside from what a detector realistically can reconstruct.

While the only analysis that would be possible in a real experimental setting is a reconstruction-level analysis, the generator-level analysis can be very useful in gaining an understanding of the dynamics of the simulated model.

3.1 PYTHIA

PYTHIA is an event generator that simulates the particle collisions and subsequent hadronization of the involved particles. PYTHIA is mainly used within LHC experimental collaborations, but is also extensively used in phenomenology studies. The probability distributions are computed using Markov Chain Monte Carlo algorithms. The hadronization process is based on the Lund String Model [42].

To simulate events with PYTHIA, a .cmnd file known as a PYTHIA card is required. This card will contain the relevant information for the event such as the number of events to be generated, which particles to collide and the center-of-mass energy, $\sqrt{s}$, of the events.

3.1.1 The Hidden Valley Module

PYTHIA is, as this is written, the only MC event generator that implements a Hidden Valley module. With the module it is possible to simulate several different HV scenarios. The scenario of interest to this work is modelled by SM-mirrored dark particles charged under a dark SU(N) gauge group that can be produced via the decay of a Z' boson. The Z' boson can also decay to SM particles, enabling the mechanisms to create semi-visible jets.

When using this module to study the dynamics and phenomenology of SU(N) dark sectors, it is of great importance to understand how the module simulates the dark sector and dark showers. PYTHIA recently received an update with significant changes to the HV module [43]. The updated version is the version 8.307 and the older version is version 8.2. This section will describe and demonstrate the parts of the HV module that are utilised in the work as well as some of the changes and new implementations introduced in the PYTHIA update to version 8.307.

For the relevant HV scenario, PYTHIA can create the 2 lightest kinds of mesons during the hadronization process; the spin-0 π_D meson and the spin-1 ρ_D meson. For the theories considered in this thesis, $m_{\pi_D} < m_{\rho_D}$. Each of the mesons can have a charge of 0, -1 or +1, resulting in 3 distinct mesons of each kind. The theory also contains spin-0 and spin-1 flavor-singlets, namely the η'_D and ω_D. In the older version of PYTHIA, the 0-charge meson and the singlet are assigned the same particle ID, or PID (`49000111` for the π^0_D and η'_D mesons and `49000113` for the ρ^0_D and ω_D mesons), while the charged mesons are assigned another PID ($\pm$`49000211` for the $\pi^\pm_D$ mesons and $\pm$`49000213` for the $\rho^\pm_D$ mesons). The consequence of this is that the 0-charge meson and the singlet must share the same properties, such as mass and decay channels. This is not a notable issue for the ρ^0_D and ω_D mesons as in general $m_{\rho_D} \approx m_{\omega_D}$. For the spin-0 case, however, the η'_D singlet mass is expected be significantly heavier than the π_D mesons in the case where $N_{f_D} \sim N_D$ [35]. Furthermore, the older version of PYTHIA does not have additional PIDs for higher flavor scenarios with additional dark mesons. This means that for an $N_{f_D} > 2$ theory, which will have more than 3 (spin-0 or spin-1) multiplet mesons, the charged mesons will also share PIDs and all charged mesons will have PID $\pm$`49000211` (or $\pm$`49000213`).

The new PYTHIA version introduces separate PIDs for the 0-charge meson and the singlet, allowing them to be non-degenerate, and additional PIDs for mesons in $N_{f_D} > 2$

theories. This feature is disabled by default, but can be enabled with the parameter setting `HiddenValley:separateFlav = on` in the PYTHIA card. Additionally, production of the η'_D singlet can be suppressed by a new parameter called `probKeepEta1`. The implementation of this parameter was validated in this work, see Section 3.1.2 below. The consequence of the number of flavors in the theory along with the flavor separation implementation will also be further illustrated in Section 3.1.2.

One of the most significant parameters in the PYTHIA card is arguably the `HiddenValley:probVector` parameter, which designates the probability of producing a spin-1 meson versus a spin-0 meson. The default value of this parameter is 0.75, meaning that the average number of spin-1 mesons produced are three times that of the produced spin-0 mesons. If a theory has very different decay modes for the π_D and ρ_D mesons, this parameter can have significant impact on the dynamics of the dark showers. Unfortunately, there is no clear theory prediction of what value of `probVector` is appropriate [35].

3.1.2 Production Probabilities of Flavor Multiplets and Singlets

In an N_{f_D} flavor theory there are $N_{f_D}^2 - 1$ (spin-0 or spin-1) flavor multiplet mesons and a singlet, i.e. $N_{f_D}^2$ mesons in total (per spin). In PYTHIA, the underlying model contains $N_{f_D}^2$ mesons, whereof N_{f_D} of these will have 0 charge and the remaining $N_{f_D}^2 - N_{f_D}$ have charge ± 1. The probability to produce any meson is the same for all mesons of the same spin, so the distribution of PIDs is expected to be even for mesons with the same spin. However, in the older version of PYTHIA or with `separateFlav = off` the 0-charge multiplet and the singlet share the same PID, and for $N_{f_D} > 2$ the charged mesons share the same PID. Thus the distribution is not always even as expected. Take $N_{f_D} = 2$ and π_D as an example. The π_D^+ and π_D^- have individual PIDs, but the π_D^0 and η'_D share a PID and therefore this PID is twice as abundant as the other PIDs. Raise N_{f_D} to 3, and there are now 3 π_D^+ that share the same PID, 3 π_D^- that share the another PID and 2 π_D^0 plus the η'_D that share a third PID, so the distribution of each PID is even. These examples are shown in Fig. 3.2.

In the new PYTHIA version with `separateFlav = on`, there is a unique PID for each kind of meson, i.e. for $N_{f_D} = 2$ there are 4 PIDs and for $N_{f_D} = 3$ there are 9. With `separateFlav = on`, each PID is as abundant as any other PID for mesons of the same spin. The PID distributions for models with $N_{f_D} = 2$ or $N_{f_D} = 3$ and `separateFlav = on` can be seen in Fig. 3.3.

The `probKeepEta1` parameter changes the probability of producing the η' singlet and the default is `probKeepEta1` = 1, which will keep the probability to produce η' equal to the probability of producing any other spin-0 meson. If the parameter is decreased, the η' production is effectively suppressed. As an example, if `probKeepEta1` is chosen to be 0.5 the abundance of η' mesons is half the abundance of any other spin-0 meson. If the parameter is set to 0, the η' signlet is not produced at all. The effect of the parameter is illustrated with PID distributions from 3 different models in Fig. 3.4. For each model, $N_{f_D} = 2$, `probVector = 0.75`, `separateFlav = On` and all dark hadrons are kept stable. The models have `probKeepEta1` either 1, 0.5 or 0. For these 3 models, the percentage of η' produced out of all dark hadrons over 50.000 simulated events are 6.60%, 3.45% and 0%, respectively.

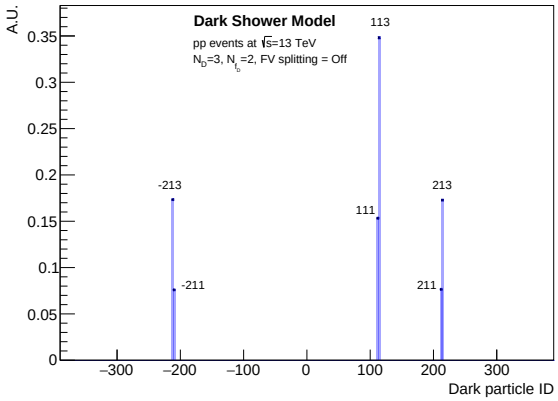

(a) $N_{f_D} = 2$ PID distribution

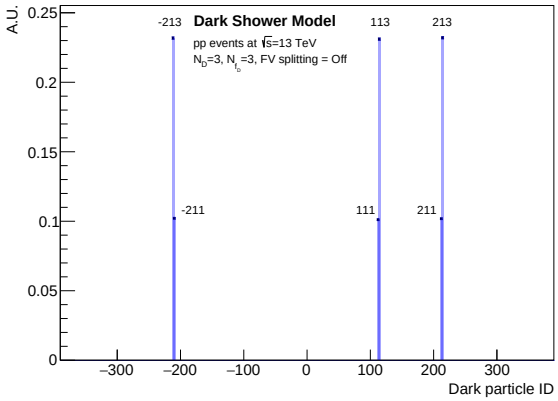

(b) $N_{f_D} = 3$ PID distribution

Figure 3.2: The dark PID distributions (without the `49000` prefix) for models in a (a) $N_{f_D} = 2$ theory or (b) $N_{f_D} = 3$ theory. `probVector = 0.75` and `separateFlav = off`. All dark particles are stable and 50.000 events are simulated.

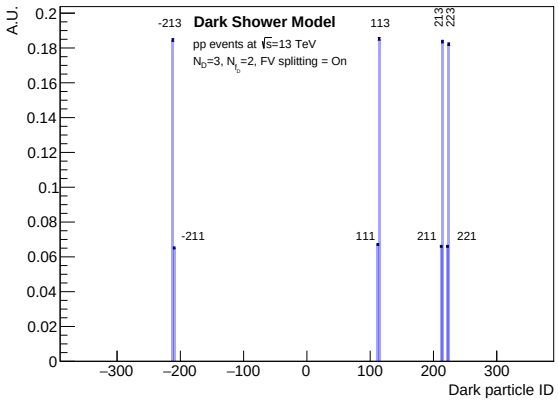

(a) $N_{f_D} = 2$ PID distribution

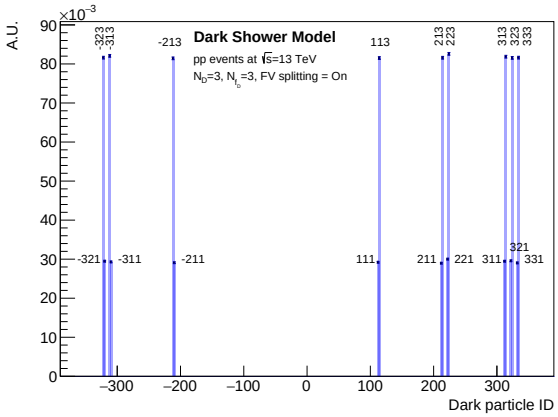

(b) $N_{f_D} = 3$ PID distribution

Figure 3.3: The dark PID distributions (without the `49000` prefix) for models in a (a) $N_{f_D} = 2$ theory or (b) $N_{f_D} = 3$ theory. `probVector = 0.75`and `separateFlav = on`. All dark particles are stable and 50.000 events are simulated.

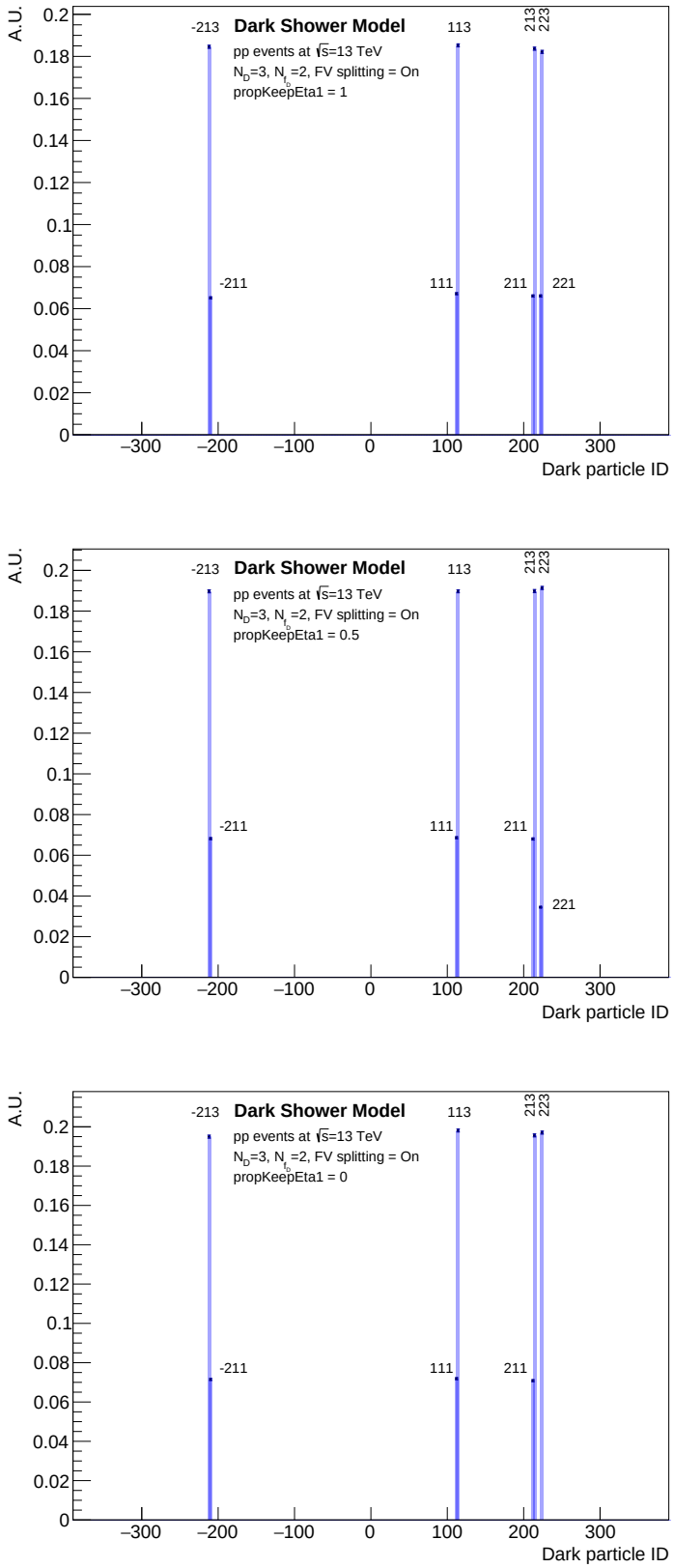

Figure 3.4: PID distribution for dark particles with various setting for `probKeepEta1` parameter over 50.000 simulated events.

3.2 DELPHES

An important step in the production of the data for the studies in this work is running the PYTHIA data output through the DELPHES program. DELPHES is a framework that simulates the detector response in a particle collision event.

Similarly to the PYTHIA card, DELPHES also requires a card in the form of a .tcl file. The information given in this card refers to the settings or abilities of the detector, such as the sensitivities, the jet clustering algorithm details and which particles are to be treated as invisible.

The output of the DELPHES analysis results in a .root file containing *branches*, a ROOT object [40]. The branches that are used the most in this work are the jet branches and the particle branch. The particle branch will contain all particles of the event. This is generator-level information and is accessible from the output file from DELPHES since DELPHES continues to store the information from the event generator. The jet branches will contain all jets of a given radius, and are given both on generator- and reconstruction-level. They reveal information about the number of jets in an event, the p_T of each jet and so on.

Throughout the work presented in this thesis, the jets are clustered with the anti-k_t algorithm with a jet radius of either $R = 0.4$ or $R = 0.8$. In the $R = 0.4$ scenario, a pre-selection cut of $p_T > 30$ GeV is applied to the jets, and for $R = 0.8$ the pre-selection cut is $p_T > 200$ GeV. In both cases the maximum pseudo-rapidity is 3; $\eta < 3$. Furthermore, it is always required that the event contains at least 2 jets that fulfill the pre-selection cuts.

4 Analysis and Discussion

4.1 Consistent Model Building

This thesis focuses on dark sector theories with a few additional over-arching requirements. Firstly, the theory of the dark sector should be a confining, QCD-like theory. Secondly, there must be some communication between the DS and the SM so we can expect to create dark particles in particle collision experiments, as well as see a signature of such events that is different from the WIMP signature. In this work, only an s-channel portal mediated by a new Z' boson is considered, but other kinds of portals exist (see e.g. Refs. [7] and [35]). Lastly, the type of phenomenology that is studied in this thesis is jetty physics, i.e. the final state of the particle collision contains jets, with both stable and unstable dark particles, and so the theory should be able to produce such phenomenology.

This frames the general structure of the theories that are of interest here, but due to the lack of strong theory priors on the details of the theories, most parameters remain essentially free or only very loosely restricted. Some examples of such parameters are the number of colors and flavors, the mass spectrum of the new particles, the mass of the new Z' boson and so on. This means that despite defining the general theory structure, there are an infinite amount of models that may be considered. It is of course an impossible task to study and search for all of them, so it's important to try to narrow down the amount of models to be considered while also maintaining a broad signature space that will maximize the discovery potential.

A lot of the recent work within this field has focused on constructing coherent benchmark models that cover the most interesting signature spaces, as in signatures that could be discovered at dark matter experiments if existent, see e.g. [7]. A central part of the work presented in this thesis revolves around the definition of a coherent set of parameters for a model that is consistent with the governing theory and coherent with recent literature in the field such as [35]. In the following section, key parameters will be discussed and important relations among them will be highlighted. Whenever possible or appropriate, limits and restrictions will be applied to the parameters.

4.1.1 Key Parameters and Their Relations

$\mathbf{N_D}$ is the number of colours of the theory. The value of this parameter has no strict theoretical restrictions except that large N_D will result in non-jetty physics. However, in this work N_D will never be larger than 8 as this is the maximum number of dark flavors

implemented in PYTHIA. This is a limitation of the simulation tool. A lower limit can also be set on N_D due to limitations of the simulation tool. PYTHIA does not include a procedure to handle the special case of $N_D = 2$ where pions and baryons are degenerate. It does have a procedure to handle non-mass degenerate (anti-)baryons and mesons relevant for an $N_D = 3$ theory, and for $N_D > 3$ such a procedure is not relevant as baryon production is mostly suppressed because they are too heavy [35]. Thus, $3 \leq N_D \leq 8$.

$\mathbf{N_{f_D}}$, the number of flavors, is another key parameter, often discussed together with N_D. This parameter dictates the number of mass-degenerate spin-0 mesons π_D and spin-1 mesons ρ_D in the theory. Given N_{f_D} there will be $N_{f_D}^2 - 1$ of each of the types of mesons as well as a spin-0 singlet η'_D and a spin-1 singlet ω_D. It is a requirement that $N_{f_D} \geq 2$, to avoid $N_{f_D}^2 - 1 = 0$ flavor multiplets, another special case not implemented in PYTHIA.

It is also important to consider the effect of different combinations of N_D and N_{f_D}, as these can have very significant consequences on the theory. The ratio of them, N_{f_D}/N_D, is an important quantity as a sufficiently large ratio will result in a scenario without confinement. A general requirement of $N_{f_D}/N_D < 3$ was proposed in Ref. [35] and will be used here.

$\mathbf{\Lambda_D}$ is the dark confinement scale. At energies above this scale, the dark sector quarks will be free, while below the scale they will confine into hadrons. Generally, there are no restrictions on this parameter, but choosing Λ_D too high can result in very little to no shower dynamics, as the dark quarks will confine immediately. With this in mind, one can set an upper bound of $\mathbf{\Lambda_D} \ll \sqrt{s}$. $\sqrt{s}$ is the center-of-mass energy of the collision, often in the order of ~ 10 TeV for LHC high-energy collisions. While this is the only strong limit on the parameter, it should not be set freely, but should be considered in relation to the masses of the dark mesons, m_{π_D} in particular. This will be elaborated below.

$\mathbf{m_{\pi_D}}$, $\mathbf{m_{\rho_D}}$, $\mathbf{m_{q_D}}$; the masses of the π_D mesons, the ρ_D mesons and the current quark mass of the dark quark q_D, are naturally also of importance when defining and discussing a model, as the masses affect the shower dynamics and multiplicities of an event. Broadly speaking, there are 2 mass hierarchy regimes; when $m_{\rho_D} < 2m_{\pi_D}$ and when $m_{\rho_D} > 2m_{\pi_D}$. The regime signifies whether the $\rho_D \to \pi_D\pi_D$ channel is closed or open. The latter case, $m_{\rho_D} > 2m_{\pi_D}$, is the kinematic threshold for this channel to be open, and it allows for ρ_D decays to DS particles only through a 2-body decay. In the former regime, $\rho_D \not\to \pi_D\pi_D$, so if ρ_D is unstable it must decay to 2 lighter SM particles only or to 2 lighter SM particles and an additional π_D meson through a 3-body decay. Such decays are theoretically realisable in e.g. $N_D = 3$ theories within the $\rho_D \not\to \pi_D\pi_D$ regime [35].

The relations between the masses and $\mathbf{\Lambda_D}$ can be determined by lattice calculations. In Ref. [35], such relations were deduced from analytical fits to lattice calculations that were presented in Ref. [44]. These relations are

$$a) \quad \frac{m_{\pi_D}}{\Lambda_D} = 5.5\sqrt{\frac{m_{q_D}}{\Lambda_D}} \qquad b) \quad \frac{m_{\rho_D}}{\Lambda_D} = \sqrt{5.76 + 1.5\frac{m_{\pi_D}^2}{\Lambda_D^2}} \tag{4.1}$$

The fit applies for small m_{π_D}/Λ_D, and remains within 10% of the lattice calculations up to $m_{\pi_D}/\Lambda_D < 2.3$. In this work, m_{π_D}/Λ_D will be kept small, and so equations 4.1a) and

b) will be used to deduce m_{q_D} and either m_{ρ_D} when m_{π_D}/Λ_D is known, or m_{π_D} when m_{ρ_D}/Λ_D is known.

$\mathbf{m_{Z'}}$, the mass of the new Z' boson, also plays a significant role in the dark shower dynamics, and is the final parameter to discuss. While there is no requirement on this parameter either, in order to achieve jetty physics $m_{Z'} \gg \Lambda_D$, approximately $m_{Z'} \geq 30\Lambda_D$ as used in Ref. [35]. This requirement will be satisfied in this work.

The limits and general requirements of the parameters argued above are summarised in Table 4.1.

Parameter	**Limits**	**Relations**
N_D	$\geq 3, \leq 8$	
N_{f_D}	≥ 2	$< 3N_D$
Λ_D	$\Lambda_D \ll \sqrt{s}$	
m_{π_D}		$m_{\pi_D} < 2.3\Lambda_D$, $m_{\pi_D} = \sqrt{\frac{m_{\rho_D}^2 - 5.76\Lambda_D^2}{1.5}}$
m_{ρ_D}		$m_{\rho_D} > \Lambda_D$, $m_{\rho_D} = \sqrt{5.76\Lambda_D^2 + 1.5 m_{\pi_D}^2}$
m_{q_D}		$m_{q_D} = 5.5^{-2} m_{\pi_D}^2 \Lambda_D^{-1}$
$m_{Z'}$		$m_{Z'} \geq 30\Lambda_D$

Table 4.1: Summary of key parameters, their limits and relations to other key parameters.

4.1.2 The r_{inv} Parameter

Under Section 2.3.1 the r_{inv} parameter was introduced as an expression of the invisibility of the dark shower and is defined as

$$r_{\text{inv}} = \left\langle \frac{N_{\text{stable dark hadrons}}}{N_{\text{stable dark hadrons}} + N_{\text{unstable dark hadrons}}} \right\rangle \tag{4.2}$$

This parameter has been extensively used in the literature since its introduction in Ref. [37], but is often mistakenly treated as a continuous parameter that defines core features of the dark shower or semi-visible jet. It must first be clarified that the r_{inv} parameter only takes on discrete values, and that the expectation value of r_{inv} is a direct consequence of the model dynamics. In theory, these dynamics can be altered and adjusted to result in any value of r_{inv}, effectively making the parameter continuous, but in practicality, only a few different scenarios are physically viable. The three primary ways to change the expected r_{inv} value in a consistent way is to adjust the number of flavors, N_{f_D}, the probability of creating spin-1 versus spin-0 mesons, i.e. `probVector` parameter, or to change the decay modes of the various mesons.

The literature generally contains very little discussion of how to determine the expected value of r_{inv} and how to handle the parameter in scenarios beyond the two basic scenarios of a dark hadron either being stable or decaying to SM particles. This should be discussed

to set a standard method of counting r_{inv} such that different research and results can easily be compared. Scenarios beyond these two will be discussed here.

In the simplest case, two things can happen to a dark hadron; it can decay to SM particles or it can remain stable. In either instance, it is clear how it should be counted towards r_{inv}. However, it is also possible that the dark hadron decays to DS particles (only) or that the dark hadron decays to both DS and SM particles, e.g. by a 3-body decay. It may seem at first glance like both of these two scenarios should count as an unstable dark hadron as it is indisputably unstable, but below arguments will be presented for the case that only the latter scenario should count towards $N_{\text{unstable dark hadrons}}$ or $N_{\text{visible particles}}$, while the former should be omitted from the calculation of r_{inv}.

Decays contained within the DS
Let the charged $\rho_D^{\pm}$ be unstable with the decay $\rho_D^{\pm} \to \pi_D^{\pm}\pi_D^0$ while all other mesons are stable. This scenario will result in $r_{\text{inv}} = 1$ since no dark mesons decay to the SM. If there is one of each dark meson in the initial state (which would be the case for `probVector` $= 0.5$), the final-state will have 3 π_D^0 (1 π_D^0 from initial state and 2 from the $\rho^{\pm}$ decays), 4 $\pi_D^{\pm}$ (1 π_D^+ and 1 π_D^- from initial state plus one of each from $\rho_D^{\pm}$ decay) and 1 ρ_D^0, which makes 8 stable dark hadrons. It is clear that for r_{inv} to be 1, $N_{\text{stable}} = N_{\text{stable}} + N_{\text{unstable}} \to N_{\text{unstable}} = 0$. For this to be true in this case, the ρ_D meson that decayed to two dark pions cannot be counted towards N_{unstable}. This would result in $r_{\text{inv}} = \frac{8}{9} < 1$, and would indicate that the shower is somewhat visible, which it clearly is not in this example.

3-body decays to both SM and DS
Let the charged $\rho_D^{\pm}$ be unstable again with the decay $\rho_D^{\pm} \to \pi_D^{\pm} + q_{SM}\bar{q}_{SM}$ while all other dark mesons are kept stable. The expected $r_{\text{inv}} \neq 1$ as there are SM particles from the DS in the final state, and so the shower cannot be fully invisible. Assuming that there are one of each dark meson in the initial state again, the final state will have 1 π_D^0, 4 $\pi_D^{\pm}$ and 1 ρ_D^0 by the same arguments as above, of course excluding the π_D^0 decay product. The number of stable dark hadrons is 6. For $r_{\text{inv}} \neq 1$ it is required that $N_{\text{stable}} < N_{\text{stable}} + N_{\text{unstable}}$, thus $N_{\text{unstable}} \neq 0$. Therefore, such decays must count towards N_{unstable}.

The conclusion is thus that, in counting r_{inv}, we must include the unstable dark hadrons when the decay product includes SM particles and exclude it when it decays exclusively to DS particles. An alternative definition of $\mathrm{r_{inv}}$ indirectly includes this rule:

$$r_{\text{inv}} = \left\langle \frac{N_{\text{invisible particles}}}{N_{\text{invisible particles}} + N_{\text{visible particles}}} \right\rangle \tag{4.3}$$

This definition also ensures a direct relation to a visible ratio r_{vis}

$$r_{vis} = \left\langle \frac{N_{\text{visible particles}}}{N_{\text{invisible particles}} + N_{\text{visible particles}}} \right\rangle$$

for which it is true that $r_{\text{inv}} = 1 - r_{vis}$. Whether the definition in 4.3 is to be preferred over 4.2 is not immediately clear and will be discussed further under section 4.4.

4.2 Kinematic Distributions of Models Below and Above the Kinematic $\rho_D \to \pi_D\pi_D$ Threshold

The behaviour difference of an SU(N_D) dark sector theory below or above the kinematic $\rho_D \to \pi_D\pi_D$ threshold is largely unexplored. 6 simple and consistent models have been constructed to expand on the understanding of the significance of the $\rho_D \to \pi_D\pi_D$ kinematic threshold. 3 of the models will be below this threshold, while 3 will be above. For each model within a mass hierarchy regime, they will differ in the number of flavors. All parameters aside from the masses and flavors will be kept the same. As a consequence, the 6 models will all have different expected values of r_{inv}, and they therefore also provide insight into the difference in kinematics of models with different dark shower visibility.

All models will be simulated in e^+e^- events at a center-of-mass energy of $\sqrt{s} = 13$ TeV. 50.000 events will be generated. All models will share these parameter values:

- $N_D = 3$
- $m_{Z'} = 1$ TeV
- $\Lambda_D = 10$ GeV
- `probVector = 0.75`
- `separateFlav = off`

They will each be assigned N_{f_D} either 2, 3 or 4. For each number of flavors, there will be a model with $m_{\pi_D} = 17$ GeV and $m_{\pi_D} = 31$ (the $m_{\rho_D} < 2m_{\pi_D}$ regime), called the *closed* model, and a model with $m_{\pi_D} = 6$ GeV and $m_{\pi_D} = 25$ (the $m_{\rho_D} > 2m_{\pi_D}$ regime), called the *open* model, thus revealing 6 distinct models.

Above the kinematic threshold the allowed decays are as follows

$$\begin{aligned} \rho_D^0 &\to \pi_D^\pm \pi_D^\mp \\ \rho_D^\pm &\to \pi_D^\pm \pi_D^0 \\ \pi_D^0 &\to q_{SM}\bar{q}_{SM} \end{aligned}$$

Below the kinematic threshold the allowed decays are as follows

$$\begin{aligned} \rho_D^0 &\to q_{SM}\bar{q}_{SM} \\ \rho_D^\pm &\to q_{SM}\bar{q}_{SM} + \pi_D^\pm \\ \pi_D^0 &\to q_{SM}\bar{q}_{SM} \end{aligned}$$

In both regimes, the $\pi_D^\pm$ is stable and is the only dark particle that adds to the invisibility of the event.

The distribution of r_{inv} from the simulations are shown in Fig. 4.1, which well illustrates the difference in r_{inv} of the 6 distinct models.

In the Figures 4.2a-4.2d jet p_T distributions of 4 different kinds can be seen; the leading jet p_T, sub-leading jet p_T, all jets p_T and the cumulative jet p_T also known as H_T. From these

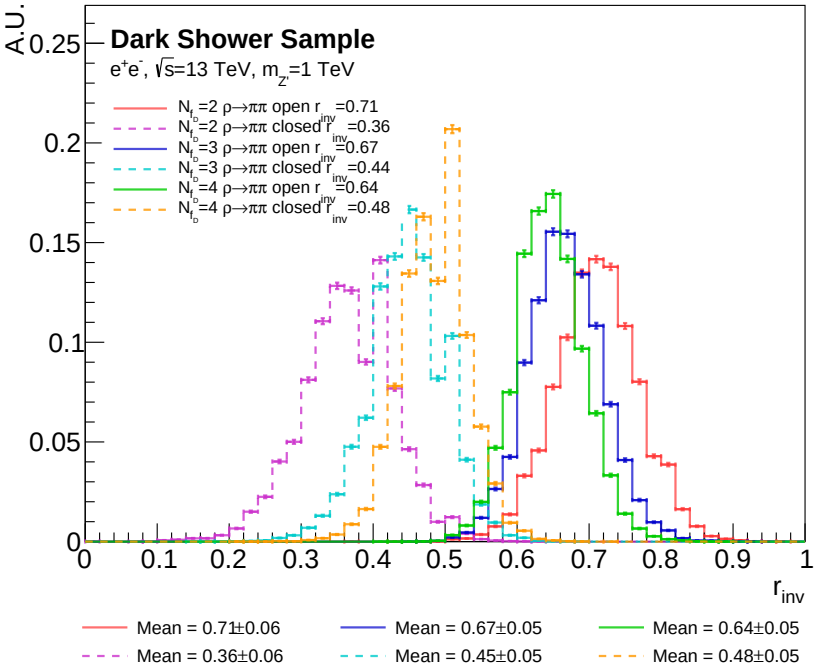

Figure 4.1: The r_{inv} distribution of the 6 distinct models.

4 plots it is clear that the jet p_T behaviour is significantly different for the open versus closed models. The closed models generally have larger jet p_T than the open models. This is no surprise as the closed models usually have more SM-decaying dark particles than the open models, as reflected in the r_{inv} distribution, and so have more visible particles that can contribute to the observed jet p_T.

It appears that the open models exhibit sharper peaks, particularly for the p_T distribution of all jets, as in Fig. 4.2c. From the left plot in this figure, which shows the jet p_T of all jets after the pre-selection cuts, it can be seen that the closed models more frequently have very high p_T jets. While the closed models have an almost even amount of $p_T \sim 800$ GeV jets and $p_T \sim 2000$ GeV jets (as well as the p_T values in between) over all events, the open models have less than half the frequency of $p_T \sim 2000$ GeV jets as that of the $p_T \sim 800$ GeV jets. Whether this difference in the peak shapes of p_T distributions is more related to the open versus closed regime or simply the visibility of the dark shower is an interesting question. All 3 open models exhibit very similar behaviours in these distributions, but they also have very small differences in the expected r_{inv} value. The largest difference in r_{inv} for the open models is 0.07, while the smallest difference in r_{inv} for a closed and open model is 0.16. The difference in the visibility of the dark shower cannot be ruled out as the origin for the difference in these p_T distribution behaviours.

Regardless of whether the model is open or closed or its invisibility, the models studied here exhibit the signatures of a dark shower. The two top figures in Fig. 4.3 show that the event is often a di-jet event and that the two leading jets are in opposite directions to each other, while the two bottom figures show that there is a significant amount of $\not{E}_T$ and that it is, for the majority of the events, closely aligned with one of the leading jets.

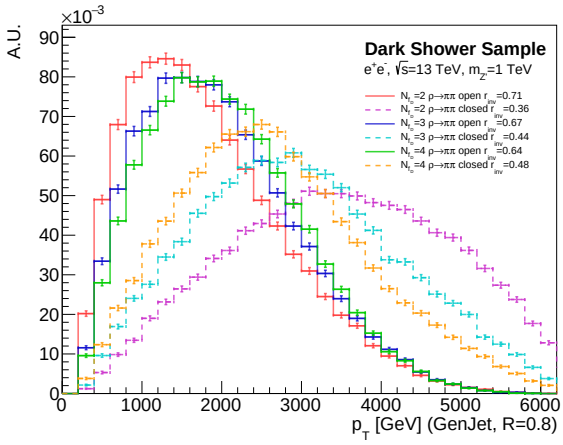

(a) The distribution of the lead jet p_T

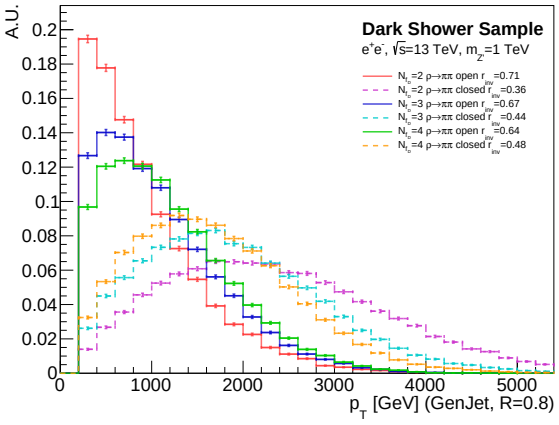

(b) The distribution of the sub-leading jet p_T

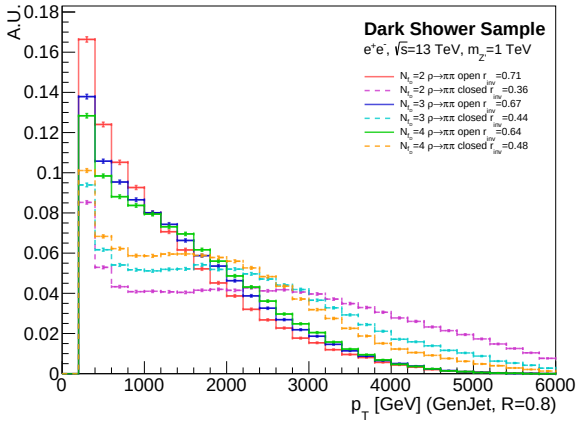

(c) The distribution of p_T of all jets

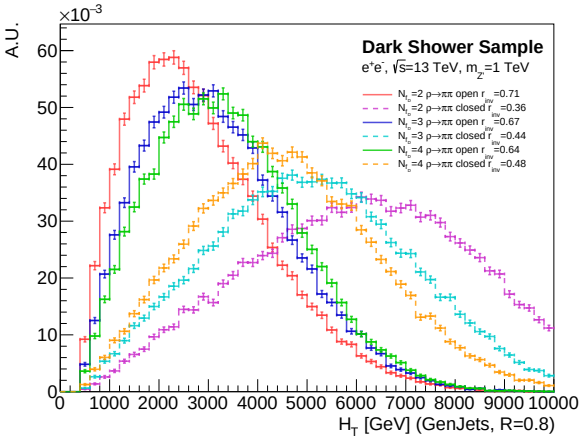

(d) The distribution of the cumulative jet p_T per event, H_T

Figure 4.2: Jet p_T distributions over 50.000 events using $R = 0.8$ jet radius.

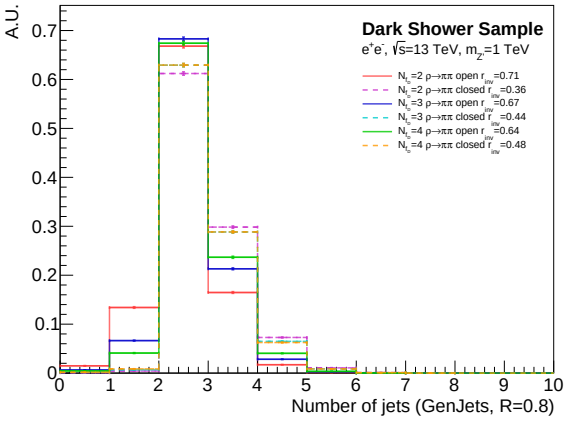

(a) The distribution of N_{jets}

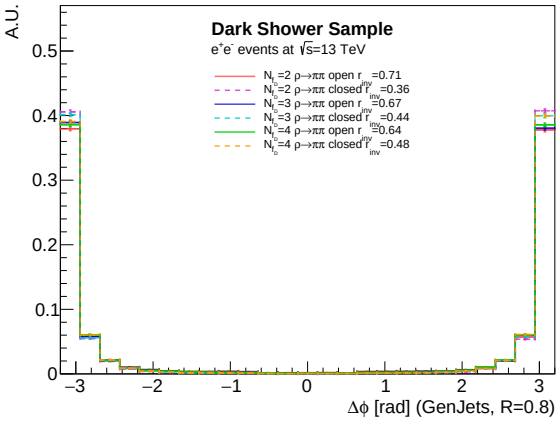

(b) The distribution of $\Delta\phi$ between the leading and sub-leading jets

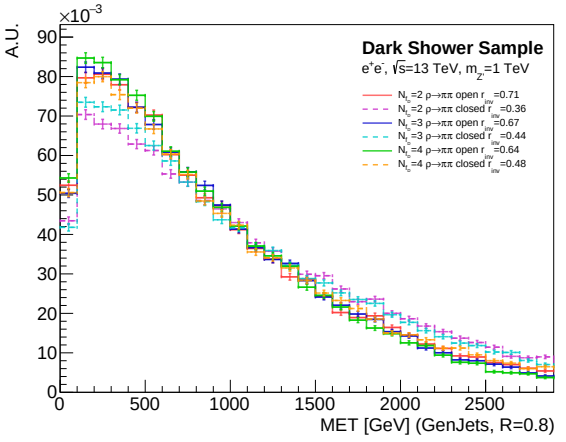

(c) The distribution of the $\not{E}_T$ of the event

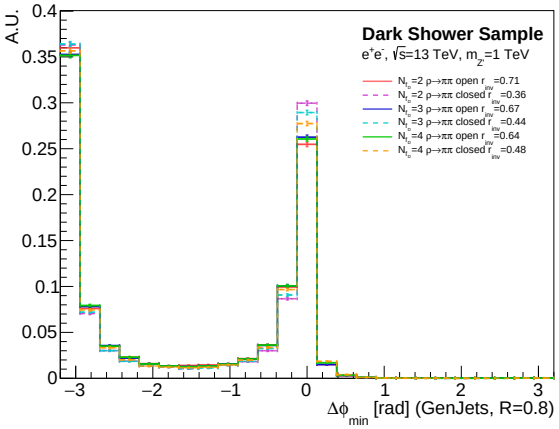

(d) The distribution of the minimum $\Delta\phi$ between the $\not{E}_T$ and either the leading or sub-leading jet

Figure 4.3: Various kinematic distributions over 50.000 events using $R = 0.8$ jet radius.

4.3 CMS Search for a Strongly-interacting Dark Sector

In Ref. [8] the CMS collaboration performed a resonance search for a Z' boson mediator coupled to a strongly-interacting dark sector. In their work, they excluded such models with $m_{Z'}$ between 1.5-4.0 TeV at a 95% confidence level. The model they used to interpret the experimental results is theoretically inconsistent with the first principles of theory and the parameter guidelines introduced earlier in Section 4.1 and generally discussed in the field [35], and consequently, the results of their work may deviate from what is expected from a model with consistent parameter settings. To understand the impact of using a model with consistent settings, a model is constructed to match the CMS benchmark values as closely as possible but within the framework introduced in Section 4.1.1.

4.3.1 The CMS Benchmark Model

The model used to interpret the results of the CMS search was based on selected benchmark values for the key parameters introduced in Section 4.1.1, whereof two parameters were varied at a time to create a 2D scan of the parameter space. Their benchmark values are summarised in Table 4.2.

In the CMS search, PYTHIA (version 3.226 and 3.230) and the HV module was used. PYTHIA (both these versions and the newer version, 3.307) is not yet built to handle a scenario with $\mathrm{N_D} = 2$ and the consequences of such a choice have not been validated. Nonetheless, CMS used this value in the PYTHIA settings for their model. In this work, $\mathrm{N_D} = 2$ will not be used but instead, $\mathrm{N_D} = 3$ will be used.

Parameter	Value	Relation
N_D	2 (3)	
N_{f_D}	2	
m_{ρ_D}	20 GeV	$m_{\rho_D} = m_{\mathrm{dark}}$
m_{π_D}	20 GeV	$m_{\pi_D} = m_{\mathrm{dark}}$
m_{q_D}	10 GeV	$\mathrm{m}_{q_D} = \frac{1}{2} m_{\mathrm{dark}}$
Λ_D	35.15 GeV	$3.2(m_{\mathrm{dark}})^{0.8}$
$\mathrm{m}_{Z'}$	3100 GeV	
probVec	0.75	
$\mathrm{r}_{\mathrm{inv}}$	0.3	

Table 4.2: Summary of CMS benchmark values and relations.

With the CMS Benchmark values of $m_{\pi_D} = 20$ GeV and $\Lambda_D = 35.15$ GeV the ratio $\mathrm{m}_{\pi_D}/\Lambda_D = 0.57$ is well below the upper limit determined for the consistent parameter settings. Hence, the relations in Eqs. 4.1a) and b) are valid, and so a fixed choice of

$m_{\rho_D} = m_{\pi_D}$ is inconsistent with lattice calculations; it can be proven that this particular choice will result in imaginary values for either Λ_D or one of the masses. These are real, physical parameters and should therefore have real values. Another unsuitable choice is setting $m_{q_D} = \frac{1}{2} m_{\pi_D}$. While this is allowed according to the Eqs. 4.1a) and b), it requires $\Lambda_D < m_{\pi_D}$, which is not fulfilled in the CMS Benchmark model.

The handling of stable and unstable dark hadrons and as an extension, the parameter $\mathrm{r_{inv}}$ in the CMS search does not represent the physically viable scenario that is expected from theory. A theory with N_{f_D} flavors will contain $\mathrm{N}_{f_D}^2$ π_D mesons and $\mathrm{N}_{f_D}^2$ ρ_D mesons (the η'_D and ω_D singlets are treated as part of these in PYTHIA), for which N_{f_D} are neutral and any number of them can decay. However, the older version of PYTHIA only has a single PID for all of the N_{f_D} neutral mesons and cannot differentiate between the individual π_D^0 or ρ_D^0 mesons. In order to make a fraction of them unstable, one must introduce a new fictitious and stable particle and let the neutral mesons decay to this particle. The new particle signifies the "stable" portion of dark mesons, it is invisible and should be treated as a final-state π_D or ρ_D meson in the analysis. Thus by adjusting the branching ratio, the fraction of unstable and stable dark mesons can be set as wished, despite the singular PID. Take $\mathrm{N}_{f_D} = 3$ as an example. PYTHIA will have 3 π_D^0 mesons, so if one wishes to have only one of these be stable, the branching ratio to the fictitious particle can be set to 0.33, which corresponds, on average, to 1 out of the 3 π_D^0 mesons being "stable".

This method is not uncommon and can be used in a theoretically consistent way, as the example with $\mathrm{N}_{f_D} = 3$ describes. However, if the branching ratios are randomly set, or varied as a continuous parameter of any value between 0 and 1, the method no longer represents the scenarios derived from the first principles of the theory. In the $\mathrm{N}_{f_D} = 3$ example, if the branching ratio of π_D^0 to the new particle is set to e.g. 0.5, it implies that 1.5 of the π_D^0 mesons are stable, but it is not expected from the theory that a meson may be partially stable.

4.3.2 Matching the CMS Benchmark to a Theoretically Consistent Model

The guiding principles for constructing a consistent model for this study is to set as many parameters as possible to the same value as the CMS benchmark, but only to the extent that it is consistent with the theoretical framework discussed in Section 4.1. If a parameter's value is inconsistent or not physically viable, it will be set to something different from the CMS benchmark values.

The number of flavors, $N_{f_D} = 2$, will not change and N_D will be set to 3 as it will for the CMS PYTHIA settings as per the mentioning earlier. Additionally, $m_{Z'}$ will remain 3.1 TeV. This will satisfy $\mathrm{m}_{Z'} \geq 30\Lambda_D$ as long as $\Lambda_D < 103$ GeV, which is a very reasonable expectation in this scenario. Since the behaviour of the parameter `probVector` in different scenarios is not well understood [35], there are no strong arguments for changing this parameter and so it will remain the same in the new model.

Some parameters that will change are the meson and quark masses. The choice of setting $\mathrm{m}_{\rho_D} = m_{\pi_D}$ poses a dilemma for choosing a comparable model, since it is impossible within the framework presented earlier to have m_{ρ_D} and m_{π_D} be the same value. A choice

must therefore be made on whether m_{ρ_D} or m_{π_D} will be equal to the CMS benchmark value. To cover the most parameter space, both of these options will be explored and thus two models will be constructed. One model will have $m_{\rho_D} = 20$ GeV, called model M-ρ, and the other model will have $m_{\pi_D} = 20$ GeV, called model M-π. The mass of the other meson, m_{π_D} and m_{ρ_D}, respectively, and the dark quark, m_{q_D}, will be determined from the relations in Eq. 4.1a) and b). To determine these masses, the value of Λ_D is also required. It is preferable to choose Λ_D equal to the CMS benchmark value if possible, however, it is only for the model M-π that $\Lambda_D = 35.15$ GeV makes sense. This results in a ρ_D meson mass of 87.84 GeV and a dark quark mass of 0.38 GeV.

For the M-ρ model it can be argued that $\Lambda_D = 8$ GeV is a sensible choice. The first argument is that the m_{π_D} should be real and non-zero, which can be realised from $m_{\pi_D} = \sqrt{\frac{m_{\rho_D}^2 - 5.76\Lambda_D^2}{1.5}}$ will require that $\Lambda_D < 8.34$. The second argument is that the model should maintain an open $\rho_D \to \pi_D\pi_D$ channel, which will allow simple 2-body decays and suppress 3-body decays of the ρ_D meson. This means that $m_{\pi_D} \leq \frac{1}{2}m_{\rho_D}$, which can be shown from the same equation sets the upper limit $\Lambda_D \geq 6.58$ GeV. This leaves only a small window of free choice for Λ_D. If $\Lambda_D = 8$ GeV the ratio m_{π_D}/Λ_D remains very close to that of the CMS benchmark (with a deviation of only 0.4%). The corresponding m_{π_D} meson mass and dark qaurk mass is 4.57 GeV and 0.087 GeV, respectively.

	Model M-ρ		Model M-π	
Parameter	**Value**	**Relation**	**Value**	**Relation**
N_D	3		3	
N_{f_D}	2		2	
m_{ρ_D}	20 GeV	$m_{\rho_D} = m_{\text{dark}}$	87.84 GeV	Eq. 4.1
m_{π_D}	4.57 GeV	Eq. 4.1	20 GeV	$m_{\pi_D} = m_{\text{dark}}$
m_{q_D}	0.087 GeV	Eq. 4.1	0.38 GeV	Eq. 4.1
Λ_D	8 GeV		35.15 GeV	
$m_{Z'}$	3100 GeV		3100 GeV	
probVec	0.75		0.75	

Table 4.3: Summary table of the parameter values and relations chosen in this work

The chosen values for the new models discussed above are summarised in Table 4.3. The parameter r_{inv} has been omitted in line with earlier discussion of this parameter. What will need to be determined instead are the decay modes of the dark hadrons. For both of the constructed models M-ρ and M-π, the $\rho_D \to \pi_D\pi_D$ channel is open. In this scenario, achieving an expected r_{inv} of 0.3, equal to the CMS benchmark value, is in fact not possible within the consistent model building framework. The lowest expected r_{inv} value of these models is $r_{\text{inv}} = \frac{5}{7}$. The reasoning is shown in the following equations and elaborated further below:

$$6\rho_D \quad \rightarrow \quad \begin{aligned} 3\rho_D^0 &\rightarrow 3\pi_D^{\pm} + 3\pi_D^{\mp} \\ 3\rho_D^{\pm} &\rightarrow 3\pi_D^{\pm} + 3\pi_D^0 \end{aligned}$$

$$2\pi_D \quad \rightarrow \quad \begin{aligned} 1\pi_D^0 + 3\pi_D^0 &\rightarrow \text{4 unstable hadrons} \\ 1\pi_D^{\pm} + 9\pi_D^{\pm} &\rightarrow \text{10 stable hadrons} \end{aligned}$$

Since `probVector` $= 0.75$, for every 2 π_D produced, 6 ρ_D are produced. The 2 π_D will consist of 1 $\pi^{\pm}$ and 1 π^0 and the 6 ρ_D of 3 $\rho_D^{\pm}$ and 3 ρ_D^0. As the $\rho_D \rightarrow \pi_D\pi_D$ channel is open, the 3 $\rho_D^{\pm}$ will decay each as $\rho_D^{\pm} \rightarrow \pi_D^{\pm}\pi_D^0$ resulting in 3 more $\pi^{\pm}$ and 3 more π^0. The 3 ρ_D^0 will decay each as $\rho_D^0 \rightarrow \pi_D^{\pm}\pi_D^{\mp}$, resulting in an additional 6 $\pi^{\pm}$. The π^0 generally cannot be kept stable by any symmetry and will decay to SM particles. Meanwhile, the $\pi^{\pm}$ are hard to not keep stable, so generally they will be the only stable dark meson in this scenario. Counting then reveals 10 $\pi^{\pm}$, i.e. 10 stable dark hadrons and 4 π^0, i.e. 4 dark hadrons decaying to the SM, and so the expected value is $r_{inv} = \frac{10}{10+4} = \frac{5}{7}$. This is actually the only viable r_{inv} value for this model (with $N_{f_D} = 2$ and $\rho_D \rightarrow \pi_D\pi_D$) when following the consistent model building principles. Due to this limitation, $r_{inv} = 0.714$ is used in the CMS PYTHIA card settings instead of the $r_{inv} = 0.3$ benchmark value.

4.3.3 Kinematic Distributions

Figures 4.4-4.7 show various kinematic distributions of the CMS benchmark model and the 2 matched models. They all show generator-level variables from 50.000 simulated events, using either jets of radius $R = 0.8$ and $p_T > 200$ GeV (the left plots) or jets of radius $R = 0.4$ and $p_T > 30$ GeV (the right plots). Fig. 4.8 shows the distribution of true r_{inv} across all events. In Appendix A additional kinematic distributions are shown.

There is no large divergence in the kinematics of the CMS Benchmark model from the theoretically consistent models, M-ρ and M-π. Nonetheless, there are interesting trends that are worth discussing.

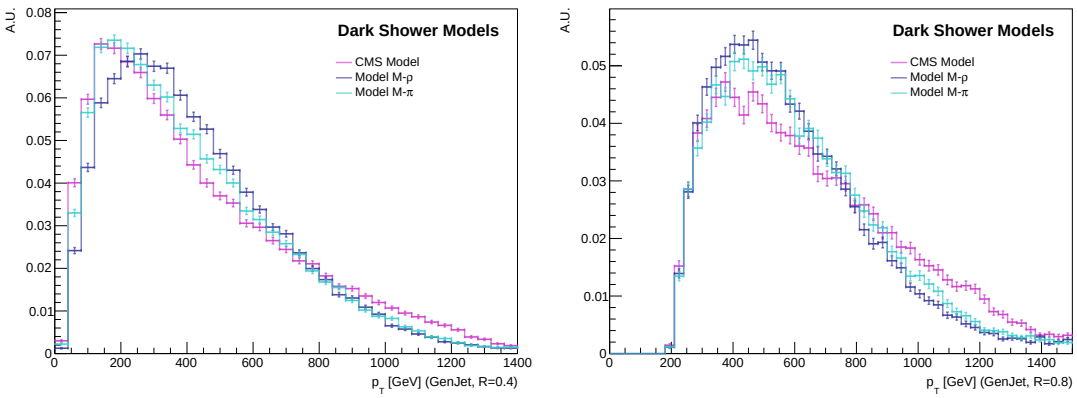

Figure 4.4: The lead jet p_T distribution with R=0.4 jets (left) and R=0.8 jets (right).

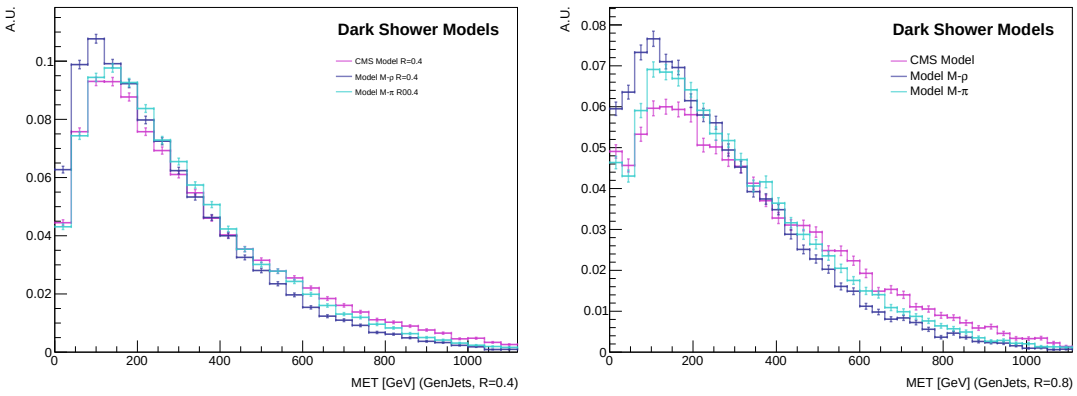

Figure 4.5: The $\not{E}_{\mathrm{T}}$ distribution with R=0.4 jets (left) and R=0.8 jets (right).

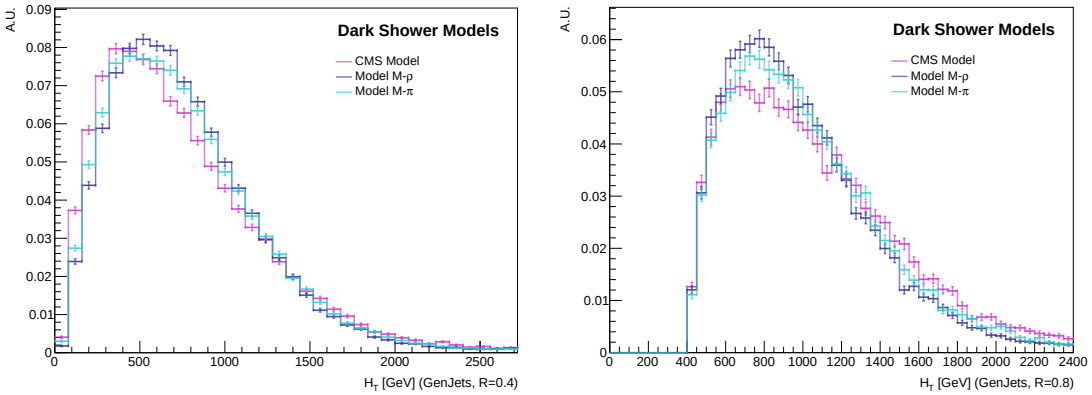

Figure 4.6: The distribution of cumulative p_T, H_T, of all jets in the event accepted by the trigger with R=0.4 jets (left) and R=0.8 jets (right).

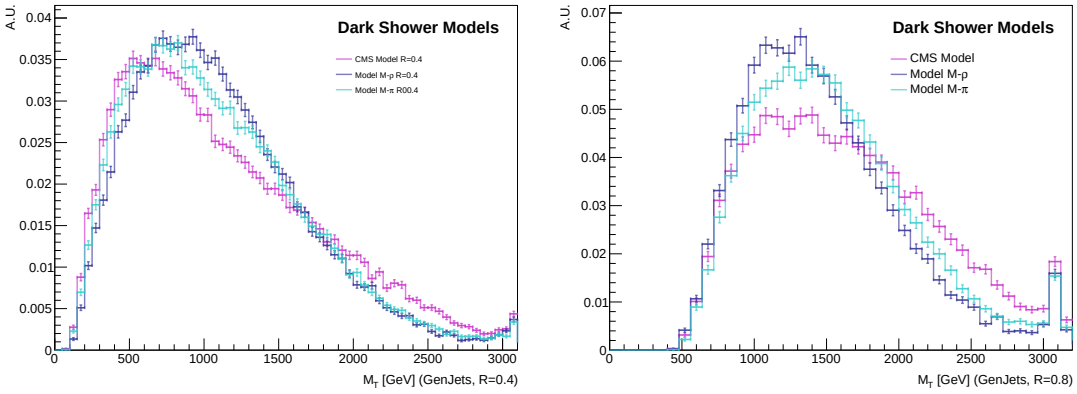

Figure 4.7: The distribution of the transverse mass determined from the leading jet, subleading jet and the $\not{E}_{\mathrm{T}}$ with R=0.4 jets (left) and R=0.8 jets (right).

Throughout all the kinematic distributions, the CMS model carries more resemblance to the M-π model than the M-ρ model, and this is generally more pronounced with $R = 0.4$ jets. As examples of this, see e.g. Figures 4.4 and 4.5. The CMS and M-π models share the values of two very important parameters, namely the mass of the SM-decaying meson

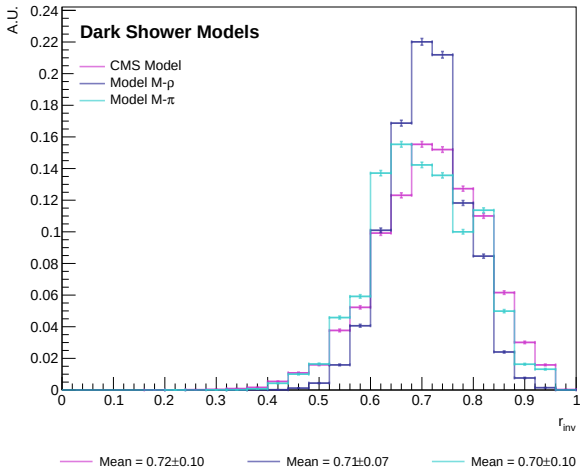

Figure 4.8: The distribution of the true value of r_{inv}.

(or mesons for the CMS model as the CMS model let both π_D and ρ_D decay) and Λ_D, whereas the M-ρ model has a much lower mass of the SM-decaying meson and a lower Λ_D. The energy and momentum transferred from the DS to the SM via the SM-decaying mesons is the only energy from the DS that will be detected (not considering $\not{E}_T$), and so it is expected that the mass of these mesons may have a more direct impact on the kinematics than the mass of the mesons that remain in the DS, which appears to be what happens according to these distributions.

These mass of the mesons, particularly the SM-decaying meson, and Λ_D are within the same order (order of 10) across all the models, and this could be a reason for the similarities in the kinematics. It must also be noted that there are several instances where the M-ρ and M-π models exhibit behaviours closer to each other than the CMS-model. In the lead jet p_T distribution in Fig. 4.4, the CMS model has a higher frequency of lead jet p_T above $\sim$ 1000 GeV than the other two models. It also shows a substantially broader peak in the M_T distribution in Fig. 4.7. These similarities are despite the relatively large difference in SM-decaying meson mass and Λ_D of these two models.

The results of this analysis indicates that within the specific DS scenario modelled here, varying the parameters such as meson masses and Λ_D within the original order of magnitude will cause slight kinematic differences, but not to a degree where the behaviours are distinctively different. Similarly, using a simplified model with direct SM-decays of all kinds of dark mesons, as opposed to more physically viable decay modes, cannot be concluded to affect the kinematics to a significant degree.

4.4 A Second Look at r_{inv}

Regardless of which definition one uses of the r_{inv} parameter, r_{inv} is a parameter that can never be directly observed (unless we manage to detect dark particles in our detectors, in which case this work is obsolete). One will quickly run into trouble with this parameter, especially if it is considered a key input parameter of the model. Nonetheless, it is an

interesting and very informative parameter to discuss, as the value of it alone can tell a lot about the phenomenology of the dark shower. It would be very exciting if we can define a parameter on reconstruction-level that is correlated with r_{inv}. An initial and perhaps naive guess is

$$N_{\text{stable}} \propto E_{\text{inv}} \quad \text{and} \quad N_{\text{unstable}} \propto E_{\text{vis}} \quad \Rightarrow \quad r_{\text{inv}} \propto E_{\text{inv}}/E_{\text{tot}}$$

where E_{inv} refers to the energy contained in the DS, E_{vis} is the visible energy, and E_{tot} refers to the sum of these. Generally it is a naive guess because it is based on the assumption that the number of particles is proportional to the energy carried by the particles, which may or may not be true. It cannot be denied that some particles may carry a large amount of energy, while others may carry very little. Additionally, the variables E_{inv} and E_{tot} implicitly refer to a single dark event, i.e. the creation and subsequent decay of a Z' into dark particles that shower and excludes any other participants of the event. For electron-positron collision events this will be the case, assuming the electron-positron annihilation results in the creation of a Z' boson and not another particle. This also means that we can easily identify E_{tot} as $\sqrt{s}$, the center-of-mass energy of the event, as we know that by conservation of energy we must get out what we put in. For proton-proton collisions the nature of the event is rarely this simple and often contains far more particles originating from various vertices and particles. To further contaminate the variable, E_{inv} should ideally not include missing energy originating from SM neutrinos, but it is impossible to identify how much of the missing energy in an event is carried by neutrinos, so this ideal case cannot be achieved.

4.4.1 Extracting $\mathrm{r_{inv}}$ on Reconstruction Level

The variable proposed as an experimentally realistic observable related to the expected value of r_{inv} has been named 'r_{inv} *reconstructed*' or r_{rec} for short, and is defined as

$$r_{\text{rec}} = \frac{\sqrt{s} - E_{\text{jets}}}{\sqrt{s}} \tag{4.4}$$

where $\sqrt{s}$ is the center-of-mass energy, and E_{jets} is the cumulative energy of all jets in the event. The performance of this variable in relating to $\mathrm{r_{inv}}$ will be tested using the 6 models introduced in Section 4.2. The 6 models have been chosen as they all have distinctively different values of expected $\mathrm{r_{inv}}$ that cover a decent range.

Figures 4.9 and 4.10 show the distribution of the variable $\mathrm{r_{rec}}$ and the event-by-event deviation from the true $\mathrm{r_{inv}}$ value, respectively. The distributions in these use reconstruction-level jets of radius $R = 0.8$ and $\mathrm{p}_T > 200$ GeV. Figure 4.11 shows the generator-level distributions of this variable, named $\mathrm{r_{gen}}$. This variable is unrealistic to measure, but is included here to show the truth-level distribution of the proposed variable as a tool to validate it. Appendix B contains the same distribution plots but for jets with radius $R = 0.4$ and $\mathrm{p}_T > 30$ GeV. The differences in these distributions between the $R = 0.4$ and $R = 0.8$ radius jets are very small and it will be sufficient to only consider one jet radius for this discussion.

The means of $\mathrm{r_{rec}}$ for the 6 different models show a clear correlation to the expected $\mathrm{r_{inv}}$ values though the means are not exactly equal to $\mathrm{r_{inv}}$. However, the mean of $\mathrm{r_{gen}}$ for

all 3 open models and 1 closed model is indeed equal to the expected r_{inv} within the uncertainty, as can be seen in Fig. 4.11. The deviation of r_{gen} from the true r_{inv} in those 4 models are on average over the 50.000 events less than 2% for each. The $N_{f_D} = 3$ and $N_{f_D} = 4$ closed models perform slightly less well.

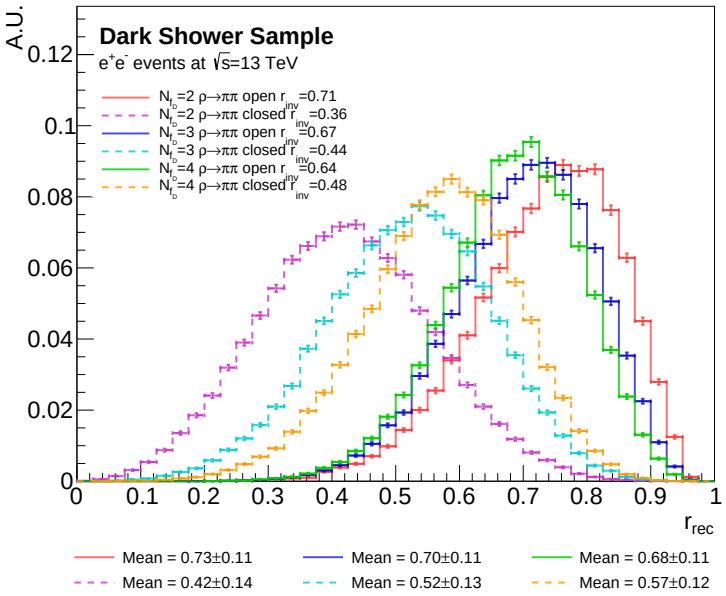

Figure 4.9: The distribution of r_{rec} for 6 different models using $R = 0.8$ jets.

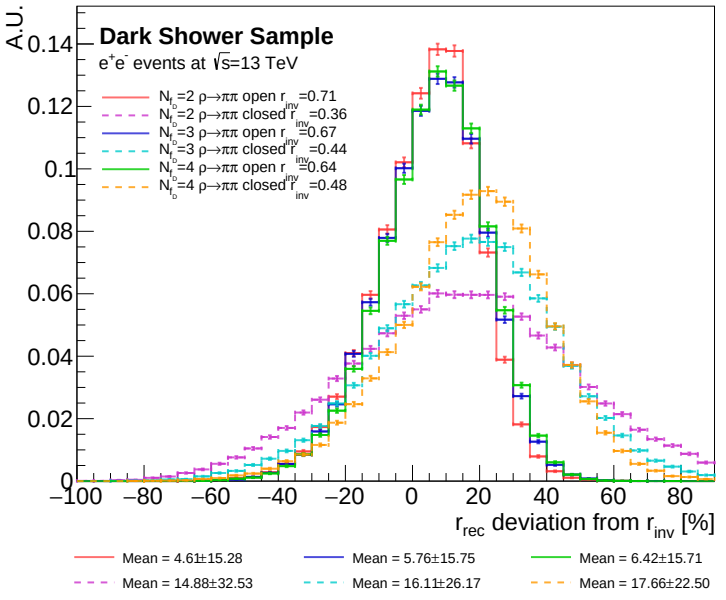

Figure 4.10: The distribution of the deviation of r_{rec} from the true r_{inv} value for 6 different models using $R = 0.8$ jets.

Across all 6 models and both distributions of r_{rec} and r_{gen}, the variable mean is larger than the expected r_{inv}. As the variable $\sqrt{s}$ is a certain and constant value in these scenarios,

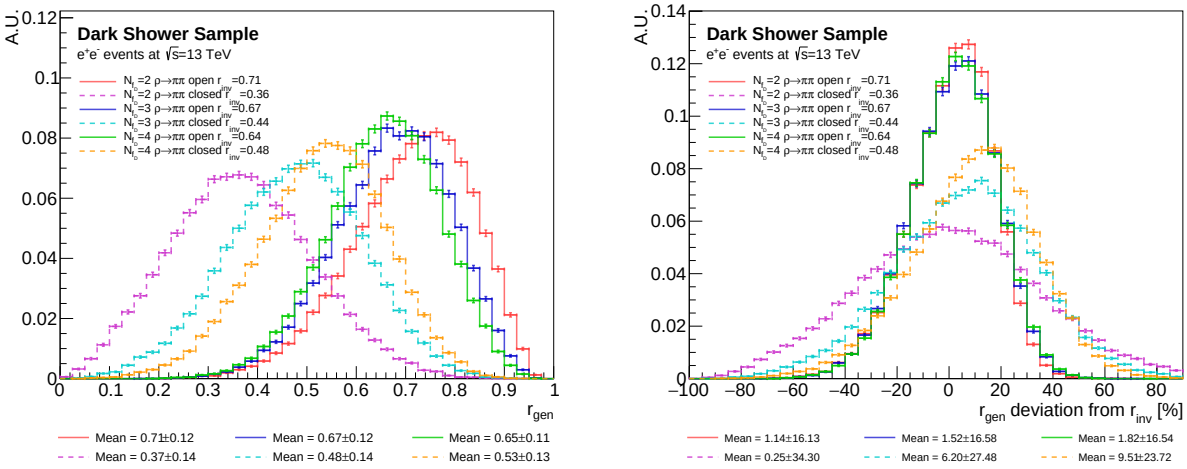

(a) The distribution of r_{gem}

(b) The distribution of the deviation of r_{gen} from the true r_{inv} value

Figure 4.11: Distribution for 6 different models using $R = 0.8$ jets.

the usually larger r_{rec} (and r_{gen}) must be due to a smaller E_{jets}. This may very well be explained by the SM neutrino background contributing to the invisible energy, while it truly belongs to the SM energy of the event. There are also many events that have a negative deviation, i.e. a lower r_{rec} (or r_{gen}) than the true r_{inv}. This could be caused by miscalculations and particularly for r_{rec}, misreconstructions of the event. However, the deviations from the true r_{inv} are sometimes, and not too rarely, too large to be suspected to originate from miscalculations. More likely, these deviations originate from a failure of the initial assumptions $N_{stable} \propto E_{inv}$ and $N_{unstable} \propto E_{vis}$ that led to the definition of the r_{rec} (and r_{gen}) variable. The assumption may not be true in all cases, but the peak in the deviation distributions, which is very sharp for the open models, and the average values of r_{rec} and r_{gen} provide support that this initial assumption is reasonable and generally a good approximation.

It is also worth noting that the expected r_{inv} values have been determined using the definition in Eq. 4.2. Using the alternative definition (Eq. 4.3), the expected r_{inv} value will always be lower, as the difference is that instead of counting an unstable dark particle as 1 in the denominator, it will count as many times as the number of SM particles it decays to, which is always ≥ 1. This would clearly mean larger deviations of r_{rec} and r_{gen} from the true r_{inv}. From these observations, the original definition of r_{inv} correlates better with the observed ratio of invisible to total energy and may therefore be preferable over the alternative definition.

5 Conclusion and Outlook

The phenomenology of dark showers is a young field with many branches of interesting collider signatures and significant discovery potential. While dark shower phenomenology has received much attention in recent years, the studies of this subject are not expansive enough to establish a wide set of clear correlations between theory and phenomenology. The work of this thesis attempts to contribute to these studies primarily through kinematic studies of semi-visible jet signatures of a QCD-like dark sector models based on the first principles of theory. There is undeniably a correlation between the visibility of the semi-visible jet and the kinematics of it. Nonetheless, this work demonstrates that the kinematics are affected by other factors, notably the decay channels of the dark hadrons and the masses of the SM-decaying dark hadrons.

Discussions of this thesis, in particular the discussion in Section 4.4, highlight an inevitable dilemma in using the variable r_{inv} as a description of the visibility of the jet and as a critical model parameter. Determining the value of this parameter assumes full knowledge of the number of dark particles in an event, which is something that we are not currently capable of measuring or will be capable of measuring in the foreseeable future. As a substitute for this variable, a new experimental observable was proposed, r_{rec}, that depends on an already common observable, namely the energy of the jets. While this substitute variable shows a great potential, its correlation to r_{inv} was only tested in e^+e^- collision events, and is expected to exhibit very different behaviour in pp collision events. Whether the variable will still be well correlated with r_{inv} is unknown, and this study could be extended directly by analysing the behaviour in pp collision events.

Similarly, the kinematic study of the models below and above the kinematic $\rho_D \to \pi_D\pi_D$ threshold could be extended to pp collision events. These studies revealed significant differences in the kinematics of the models, but was not able to conclude if these differences originated from the variation of the visibility of the semi-visible jets or the distinctive dynamics, such as 3-body decays being introduced in the closed models. It is also likely to be caused by a combination of both factors. This hypothesis could be tested by studying additional models, and perhaps it would be most productive to study models that share a very similar visibility, but varies in the dynamics and decay channels. While raising the number of flavors will close the gap between the expected value of r_{inv} of the open and closed models, the minimum difference achievable by only changing N_{f_D} is $\Delta(r_{inv})_{min} = 0.072$, which occurs for $N_{f_D} = 8$, the maximum number of flavors currently implemented in PYTHIA. However, by also varying the `probVector` parameter between models, it's possible to minimize this gap even further, but it introduces `probVector` as a new unknown that may contribute to kinematic differences in its own way.

The kinematic studies of the CMS Benchmark model and the comparable models that were defined in consistency with the theory principles, did not reveal any significant deviations. The scope of the models studied in this work are very limited; they assume an open $\rho_D \to \pi_D\pi_D$ channel and consists of only one expected r_{inv} value or a very limited span of visibility. The proposed models may cover very little signature parameter space, and there are plenty of opportunities within the consistent theory framework to propose additional comparable models. A variable that may be particularly interesting to vary is the `probVector`. As discussed previously, there is no strong prior for what this parameter should be, and in this study it was simply chosen to match the CMS Benchmark.

Some final remarks on the use of the PYTHIA simulation tools are appropriate. The new options for separating the flavors as well as suppressing the η'_D singlet production were not applied to any of the models of this thesis. Exploring the impact of these new simulation mechanisms could be of great interest. While the mechanisms have been validated, they are new and very little is known about how their implementations will affect the model behaviours. This is an obvious possible direction for future studies of dark shower phenomenology.

In conclusion, this thesis has only covered a very limited scope of dark shower phenomenology. It is clear that kinematic studies available at this time are far from exhaustive, and the possibilities for extending the studies in this thesis, and of dark shower phenomenology in general, are almost endless. This thesis addresses some specific models and questions, and provides motivation for continuing the studies of dark showers for present and future colliders.

References

[1] Butterworth, J. The standard model: How far can it go and how can we tell? **374**, 20150260. URL http://arxiv.org/abs/1601.02759. 1601.02759.

[2] Planck Collaboration. Planck 2018 results. VI. cosmological parameters **641**, A6. URL http://arxiv.org/abs/1807.06209. 1807.06209[astro-ph].

[3] Cumming, R. Därför glömde alla Knut Lundmarks stora upptäckt: den mörka materian - Populär Astronomi. URL https://www.popularastronomi.se/2015/06/darfor-glomde-alla-knut-lundmarks-stora-upptackt-den-morka-materian/.

[4] Strassler, M. J. & Zurek, K. M. Echoes of a hidden valley at hadron colliders **651**, 374–379. URL http://arxiv.org/abs/hep-ph/0604261. hep-ph/0604261.

[5] Bernreuther, E., Kahlhoefer, F., Krämer, M. & Tunney, P. Strongly interacting dark sectors in the early universe and at the LHC through a simplified portal URL http://arxiv.org/abs/1907.04346. 1907.04346.

[6] Cohen, T., Doss, J. & Freytsis, M. Jet substructure from dark sector showers **2020**, 118. URL http://arxiv.org/abs/2004.00631. 2004.00631.

[7] Knapen, S., Shelton, J. & Xu, D. Perturbative benchmark models for a dark shower search program **103**, 115013. URL http://arxiv.org/abs/2103.01238. 2103.01238.

[8] CMS Collaboration. Search for resonant production of strongly-coupled dark matter in proton-proton collisions at 13 TeV. URL https://cds.cern.ch/record/2778946. Number: CMS-PAS-EXO-19-020.

[9] Pich, A. The standard model of electroweak interactions. URL http://arxiv.org/abs/1201.0537. Type: article, 1201.0537[hep-ex,physics:hep-ph].

[10] Particle data group. URL https://pdg.lbl.gov/.

[11] Putting the pauli exclusion principle on trial. URL https://cerncourier.com/a/putting-the-pauli-exclusion-principle-on-trial/.

[12] FASER neutrino detector | FASER: ForwArd search ExpeRiment at the LHC. URL https://faser.web.cern.ch/about-the-experiment/detector-design/fasernu.

[13] Abreu, H. *et al.* First neutrino interaction candidates at the LHC **104**, L091101. URL https://link.aps.org/doi/10.1103/PhysRevD.104.L091101.

[14] Abreu, H. *et al.* Detecting and studying high-energy collider neutrinos with FASER at the LHC: FASER collaboration **80**, 61. URL http://link.springer.com/10.1140/epjc/s10052-020-7631-5.

[15] Anchordoqui, L. & Halzen, F. Lessons in particle physics URL http://arxiv.org/abs/0906.1271. 0906.1271.

[16] Altarelli, G. & Wells, J. QCD: The theory of strong interactions. In Altarelli, G. & Wells, J. (eds.) *Collider Physics within the Standard Model: A Primer*, Lecture Notes in Physics, 27–96 (Springer International Publishing). URL https://doi.org/10.1007/978-3-319-51920-3_2.

[17] Chaudhuri, A. K. A short course on relativistic heavy ion collisions. URL http://arxiv.org/abs/1207.7028. Type: article, 1207.7028[hep-ph,physics:nucl-th].

[18] Krohn, D., Thaler, J. & Wang, L.-T. Jet trimming **2010**, 84. URL http://arxiv.org/abs/0912.1342. 0912.1342[hep-ph].

[19] Ellis, S. D., Huston, J., Hatakeyama, K., Loch, P. & Toennesmann, M. Jets in hadron-hadron collisions **60**, 484–551. URL http://arxiv.org/abs/0712.2447. 0712.2447[hep-ph].

[20] Cacciari, M., Salam, G. P. & Soyez, G. The anti-k_t jet clustering algorithm **2008**, 063–063. URL http://arxiv.org/abs/0802.1189. 0802.1189[hep-ph].

[21] Peter, A. H. G. Dark matter: A brief review URL http://arxiv.org/abs/1201.3942. 1201.3942.

[22] Ostriker, J. P. & Peebles, P. J. E. A numerical study of the stability of flattened galaxies: or, can cold galaxies survive? **186**, 467–480. URL https://ui.adsabs.harvard.edu/abs/1973ApJ...186..467O. ADS Bibcode: 1973ApJ...186..467O.

[23] Ostriker, J. P., Peebles, P. J. E. & Yahil, A. The size and mass of galaxies, and the mass of the universe **193**, L1. URL https://ui.adsabs.harvard.edu/abs/1974ApJ...193L...1O. ADS Bibcode: 1974ApJ...193L...1O.

[24] Einasto, J., Kaasik, A. & Saar, E. Dynamic evidence on massive coronas of galaxies **250**, 309–310. URL https://www.nature.com/articles/250309a0. Number: 5464 Publisher: Nature Publishing Group.

[25] Steigman, G. & Turner, M. S. Cosmological constraints on the properties of weakly interacting massive particles **253**, 375–386. URL https://ui.adsabs.harvard.edu/abs/1985NuPhB.253..375S. ADS Bibcode: 1985NuPhB.253..375S.

[26] Brandt, T. D. CONSTRAINTS ON MACHO DARK MATTER FROM COMPACT STELLAR SYSTEMS IN ULTRA-FAINT DWARF GALAXIES **824**, L31. URL https://iopscience.iop.org/article/10.3847/2041-8205/824/2/L31.

[27] Tisserand, P. *et al.* Limits on the macho content of the galactic halo from the EROS-2 survey of the magellanic clouds **469**, 387–404. URL https://ui.adsabs.harvard.edu/abs/2007A&A...469..387T/abstract.

[28] Agnese, R. *et al.* Search for low-mass WIMPs with SuperCDMS **112**, 241302. URL http://arxiv.org/abs/1402.7137. 1402.7137[astro-ph,physics:hep-ex,physics:physics].

[29] Akerib, D. S. *et al.* Results from a search for dark matter in the complete LUX exposure **118**, 021303. URL http://arxiv.org/abs/1608.07648. 1608.07648[astro-ph,physics:hep-ex,physics:physics].

[30] Aprile, E. *et al.* Dark matter search results from a one tonne$\times$year exposure of XENON1t **121**, 111302. URL http://arxiv.org/abs/1805.12562. 1805.12562[astro-ph,physics:hep-ex,physics:hep-ph,physics:physics].

[31] Amare, J. *et al.* Annual modulation results from three-year exposure of ANAIS-112 **103**, 102005. URL http://arxiv.org/abs/2103.01175. 2103.01175[astro-ph,physics:hep-ex].

[32] Han, T., Si, Z., Zurek, K. M. & Strassler, M. J. Phenomenology of hidden valleys at hadron colliders **2008**, 008–008. URL http://arxiv.org/abs/0712.2041. 0712.2041[hep-ph].

[33] Beauchesne, H., Bertuzzo, E. & Grilli di Cortona, G. Dark matter in hidden valley models with stable and unstable light dark mesons **2019**, 118. URL https://doi.org/10.1007/JHEP04(2019)118.

[34] Cohen, T., Lisanti, M., Lou, H. K. & Mishra-Sharma, S. LHC searches for dark sector showers **2017**, 196. URL http://arxiv.org/abs/1707.05326. 1707.05326.

[35] Doglioni, C., Hemme, N., Kulkarni, S. *et al.* Theory, phenomenology, and experimental avenues for dark showers: a snowmass 2021 report URL http://arxiv.org/abs/2203.09503. 2203.09503.

[36] Bernardi, G. & Konigsberg, J. The higgs boson search and discovery. In *The Standard Theory of Particle Physics*, vol. Volume 26 of *Advanced Series on Directions in High Energy Physics*, 275–313 (WORLD SCIENTIFIC). URL https://www.worldscientific.com/doi/10.1142/9789814733519_0015.

[37] Cohen, T., Lisanti, M. & Lou, H. K. Semi-visible jets: Dark matter undercover at the LHC **115**, 171804. URL http://arxiv.org/abs/1503.00009. 1503.00009.

[38] Bierlich, C. *et al.* A comprehensive guide to the physics and usage of PYTHIA 8.3 URL http://arxiv.org/abs/2203.11601. 2203.11601.

[39] de Favereau, J. *et al.* DELPHES 3, a modular framework for fast simulation of a generic collider experiment **2014**, 57. URL http://arxiv.org/abs/1307.6346. 1307.6346.

[40] ROOT: ROOT reference documentation. URL https://root.cern/doc/v612/.

[41] Hemme, N., Nair, H., Singh, A. & Albouy, G. NHemme/dark-showers-22. URL https://github.com/NHemme/dark-showers-22. Original-date: 2021-11-29T10:36:34Z.

[42] Andersson, B., Gustafson, G., Ingelman, G. & Sjöstrand, T. Parton fragmentation and string dynamics **97**, 31–145. URL https://linkinghub.elsevier.com/retrieve/pii/0370157383900807.

[43] PYTHIA 8.3 - PYTHIA 8.3. URL https://pythia.org/.

[44] Fischer, C. S. Infrared properties of QCD from dyson-schwinger equations **32**, R253–R291. URL http://arxiv.org/abs/hep-ph/0605173. hep-ph/0605173.

A More Kinematic Distributions for Section 4.3

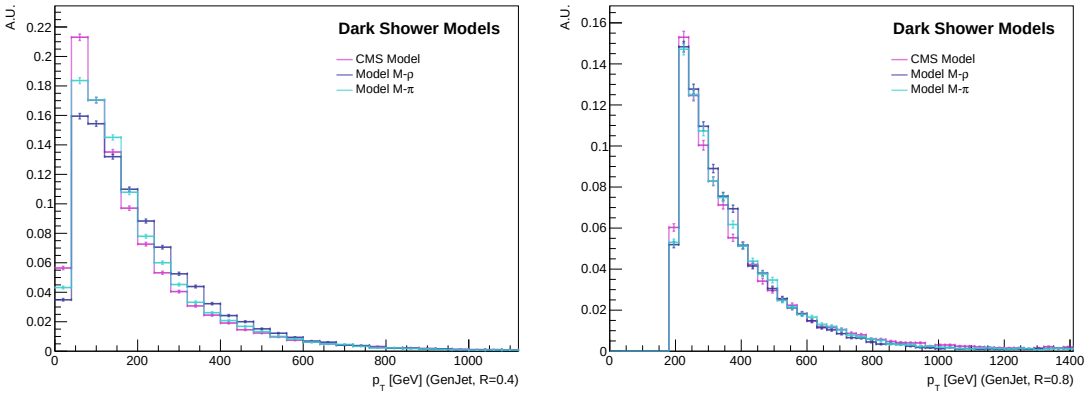

Figure A.1: The sub-leading jet p_T distribution with R=0.4 jets (left) and R=0.8 jets (right).

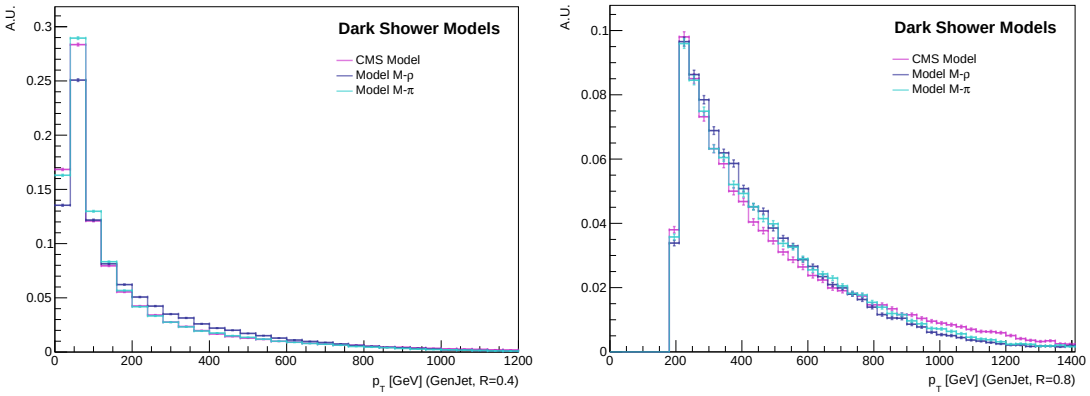

Figure A.2: The distribution of p_T of all jets fulfilling pre-selection requirements in the events with R=0.4 jets (left) and R=0.8 jets (right).

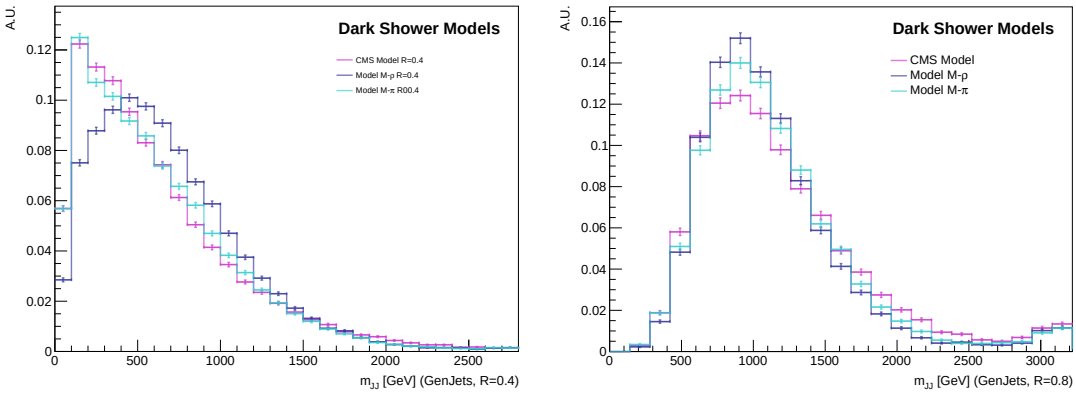

Figure A.3: The distribution of the invariant mass determined from the leading and sub-leading jet with R=0.4 jets (left) and R=0.8 jets (right).

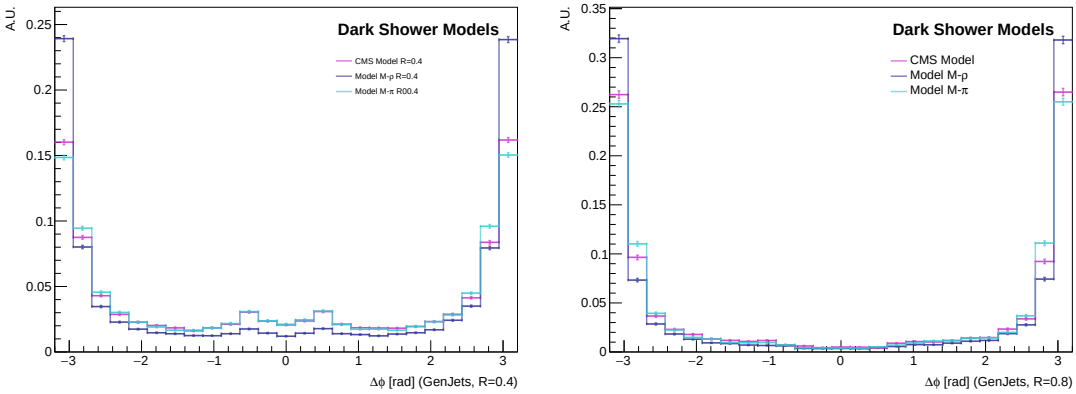

Figure A.4: The distribution of $\Delta\phi$ between the leading and sub-leading jet with R=0.4 jets (left) and R=0.8 jets (right).

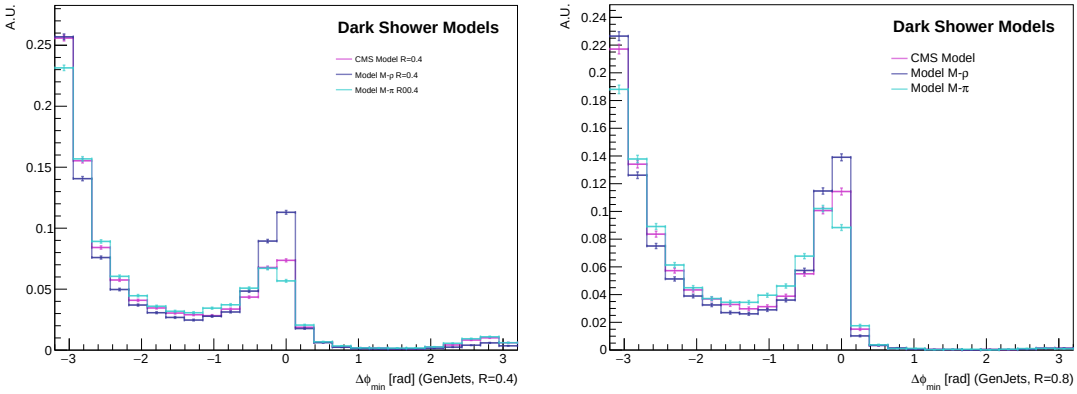

Figure A.5: The distribution of $\Delta\phi_{\text{min}}$ between the $\not{E}_{\text{T}}$ and leading or sub-leading jet with R=0.4 jets (left) and R=0.8 jets (right).

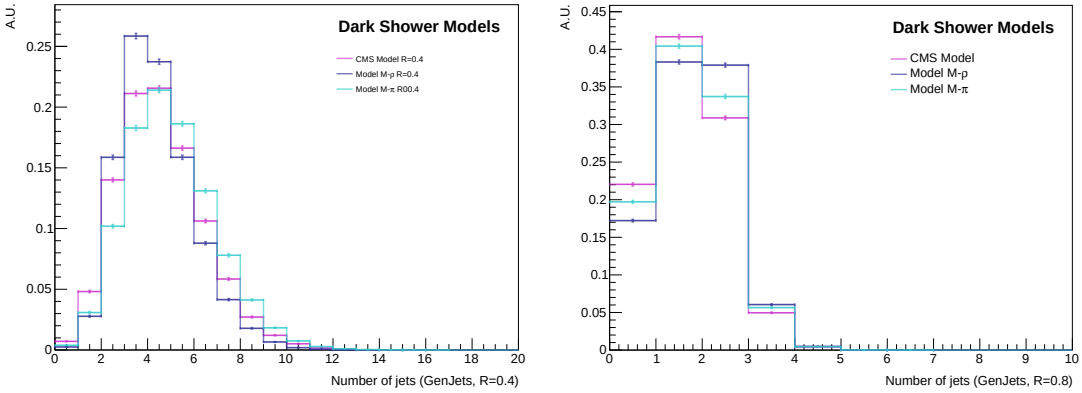

Figure A.6: The distribution of N_{jets} per event ith R=0.4 jets (left) and R=0.8 jets (right) (note that the jets included in this variable do not need to fulfill the pre-selection requirements).

B Distributions of r_{rec} and r_{gen} with R=0.4 jets

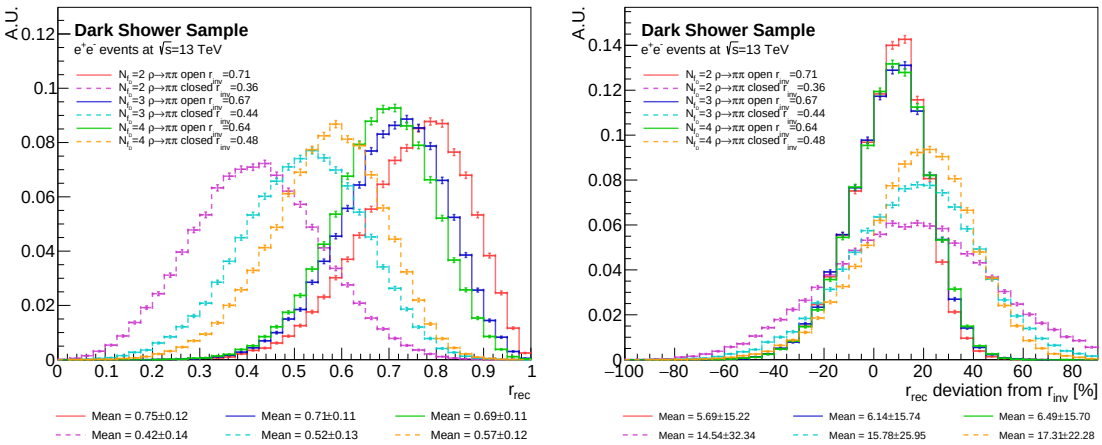

Figure B.1: The distribution of r_{rec} for 6 different models using $R = 0.4$ jets (right) and the distribution of the deviation of r_{rec} from the true r_{inv} value for 6 different models using $R = 0.4$ jets (left).

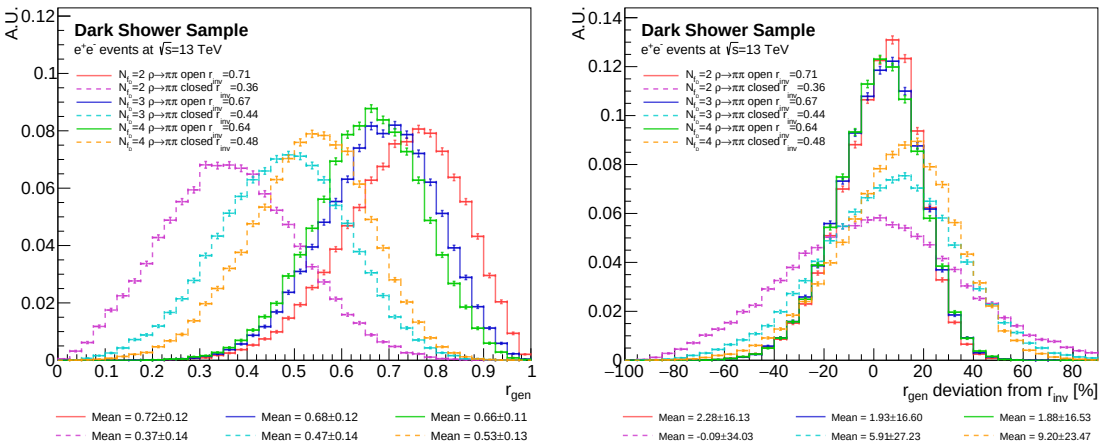

Figure B.2: The distribution of r_{gen} for 6 different models using $R = 0.4$ jets (right) and the distribution of the deviation of r_{gen} from the true r_{inv} value for 6 different models using $R = 0.4$ jets (left).